Pharmacological Targeting of the NLRP3 trLRR Domain with Isothiazolinones Overcomes CRID3-Resistant Inflammation

Hawon Woo[1*], Yeonseo Jang[1*], Soyeon Kim[1], Wonyoung Kim[1], Fenfen Zhang[2], Raghvendra Mall[3], Chirag N. Patel[3,4], Melan Kurera[5], Chinh Ngo[5], Simon H. Jiang[5], Asia Nicotra[6], Bénédicte F. Py[6], Min Zheng[2**], Si Ming Man[5**], Rajendra Karki[1**]

[1] Department of Biological Sciences, College of Natural Science, Seoul National University, Seoul, 08826, South Korea.

[2] Institute of Infectious Diseases, Shenzhen Bay Laboratory, Shenzhen, Guangdong, 518132, China.

[3] Biotechnology Research Center, Technology Innovation Institute, P.O. Box:9639, Abu Dhabi, United Arab Emirates.

[4] Translational Gerontology Branch, National Institute on Aging, NIH, Baltimore, MD, USA.

[5] Division of Immunology and Infectious Diseases, The John Curtin School of Medical Research, The Australian National University, Canberra, Australia.

[6] CIRI, Centre International de Recherche en Infectiologie, Univ Lyon, Inserm, U1111, Université Claude Bernard Lyon 1, CNRS, UMR5308, ENS de Lyon, F-69007, Lyon, France

**Corresponding author. Email: rkarki@snu.ac.kr (RK); Email: siming.man@anu.edu.au (SMM); Min Zheng. Email: min.zheng@szbl.ac.cn (MZ)

*These authors contributed equally to this work.

Abstract

The NLRP3 inflammasome is a key driver in inflammatory, infectious, metabolic, and neurodegenerative diseases. Although the NLRP3 inhibitor CRID3 (also known as MCC950) exhibits potent activity, it cannot inhibit several hyperactive NLRP3 mutations associated with autoinflammatory syndromes and has not progressed clinically, underscoring the need for the development of new NLRP3 inhibitors. Through a high-throughput screen, we identified LOC14, an isothiazolinone-containing small molecule, as a selective NLRP3 inhibitor. Distinct from CRID3, which targets the NACHT domain, LOC14 binds to or near the LRR domain of NLRP3 and inhibits both CRID3-responsive and CRID3-non-responsive hyperactive or gain-of-function NLRP3 variants. Furthermore, we identified that the carbonyl oxygen of the isothiazol-3(2H)-one moiety is critical for inhibitory activity. In mice, LOC14 exerted anti-inflammatory effects in skin inflammation, intestinal inflammation, and sepsis, demonstrating broad physiological and therapeutic relevance. Our findings highlight isothiazolinone-containing compounds as first-in-class NLRP3 inhibitors for use against inflammatory diseases.

Introduction

The innate immune system responds to various pathological conditions through the orchestration of highly specialized protein signaling complexes, ensuring host defense and tissue homeostasis. Central to this response is the inflammasome, a multi-protein complex that is assembled in response to pathogen-associated molecular patterns (PAMPs) or damage-associated molecular patterns (DAMPs) (Gurung, 2025; Karki & Kanneganti, 2019; Lamkanfi & Dixit, 2014; Swanson *et al*, 2019). Once activated, the inflammasome triggers activation of caspase-1, which cleaves the pro-inflammatory cytokines pro-IL-1β and pro-IL-18 into their mature, biologically active forms. Caspase-1 activation also cleaves gasdermin D (GSDMD), allowing its N-terminal fragment to translocate to the plasma membrane (Kayagaki *et al*, 2015; Shi *et al*, 2015), where it forms pores and facilitates the release of certain cytokines and cellular contents, ultimately leading to an inflammatory form of cell death called pyroptosis (Karki & Kanneganti, 2021; Man & Kanneganti, 2024).

Among the various inflammasomes, the NLRP3 inflammasome has garnered global attention in fundamental and translational science due to its ability to sense a diverse array of PAMPs and DAMPs and trigger inflammation and cell death in multiple disease contexts (Anand, 2025; Hollis & Lukens, 2025; Li *et al*, 2025; Pandey *et al*, 2025; Xu & Nunez, 2023). NLRP3 activation is tightly regulated by a sequence of priming and activation events. The priming phase is driven by signals that activate the signaling proteins nuclear factor-kappa B (NF-κB) and extracellular signal-regulated kinase (ERK), leading to the upregulation of NLRP3 and pro-IL-1β (Bauernfeind *et al*, 2009; Franchi *et al*, 2009). The subsequent activation phase requires conformational changes in NLRP3 that facilitate the interaction between NLRP3 and the serine/threonine kinase NEK7 (He *et al*, 2016; Schmid-Burgk *et al*, 2016; Shi *et al*, 2016). This interaction is pivotal for the recruitment and oligomerization of the adaptor

protein ASC, culminating in the assembly of the NLRP3 inflammasome (Sharif *et al*, 2019).

The NLRP3 inflammasome is implicated in various infectious and inflammatory diseases (Vande Walle & Lamkanfi, 2024). Gain-of-function mutations in NLRP3 cause the development of a group of inflammatory diseases known as cryopyrin-associated periodic syndromes, characterized by severe localized and systemic inflammation and clinical manifestations owing to aberrant inflammasome activation and excessive IL-1β secretion (Aganna *et al*, 2002; Feldmann *et al*, 2002; Hoffman *et al*, 2001). Beyond genetic predispositions, NLRP3 activation triggered by cholesterol crystals and monosodium urate crystals leads to the progression of atherosclerosis (Martinon *et al*, 2006) and gout (Duewell *et al*, 2010), respectively. Moreover, the NLRP3 inflammasome is activated by protein fibrils and aggregates, β-amyloid plaques, and tau fibers, contributing to the pathogenesis of Alzheimer's disease (Heneka *et al*, 2013). Despite the therapeutic importance of targeting the NLRP3 inflammasome, the development of effective inhibitors has faced considerable challenges. Several CRID3-based second-generation NLRP3 inhibitors have been developed, but none have received clinical approval (Coll & Schroder, 2025; Mangan *et al*, 2018), and many cannot inhibit several NLRP3 variants associated with autoinflammatory syndromes (Cosson *et al*, 2024; Feng *et al*, 2025; Kim *et al*, 2025; Vande Walle *et al*, 2019).

In this study, we used a chemical compound screen to identify the small-molecule LOC14 as an inhibitor of NLRP3. LOC14 bound to the transition LRR domain of NLRP3 and disrupted NLRP3-NEK7 interaction. We identified isothiazolinone as the functional group of LOC14, inhibiting the NLRP3 inflammasome and pyroptosis. Notably, LOC14 did not inhibit the activation of NLRP1, AIM2, NLRC4, and Pyrin inflammasomes. In mouse models of psoriasis, colitis, and sepsis, administration of LOC14 or isothiazolinone suppressed inflammatory responses and improved disease outcomes.

Overall, our findings highlight LOC14 and isothiazolinone as promising therapeutic agents for treating NLRP3-associated inflammatory and infectious diseases.

Results

A chemical library screen reveals LOC14 as an inhibitor of the NLRP3 inflammasome

We screened a chemical library of 1,140 compounds in primary bone marrow-derived macrophages (BMDMs) treated with the NLRP3 activator combination, lipopolysaccharide (LPS) plus nigericin, and assessed for cell death to identify potential inhibitors of the NLRP3 inflammasome (**Fig. 1A**). The top five inhibitors in order of the highest potency were the sulfonylurea NLRP3 inhibitor CRID3 (also known as MCC950), LOC14, the steroidal lactone Withaferin A, the caspase-1 dipeptide inhibitor Belnacasan, and the NF-κB inhibitor NF-κB-IN-1 (also known as 1,6-Heptadiene-3,5-dione) (**Fig. 1B**). Of these candidates, LOC14 is not known to inhibit NLRP3 previously, whereas CRID3 (Coll *et al*, 2015), Belnacasan (Wannamaker *et al*, 2007), NF-κB-IN-1(Yin *et al*, 2018) and Withaferin A (Kim *et al*, 2015) have been reported to inhibit NLRP3 inflammasome activation.

To validate the role of the new candidate LOC14 in suppressing NLRP3 inflammasome activation, we stimulated wild-type (WT) and *Nlrp3*$^{-/-}$ BMDMs with the NLRP3 activators LPS plus nigericin or LPS plus ATP, in the presence or absence of LOC14 or CRID3. Both LOC14 and CRID3 abolished cell death in WT BMDMs induced by LPS plus nigericin or LPS plus ATP (**Fig. 1C, D, Supplementary Fig. 1A, B**). The cell death inhibitory effect of LOC14 in WT BMDMs was comparable to the outcome achieved in *Nlrp3*$^{-/-}$ BMDMs (**Fig. 1C, D, Supplementary Fig. 1A, B**). Following NLRP3 inflammasome activation, both the cysteine protease caspase-1 and pore-forming protein GSDMD undergo proteolytic cleavage (Kayagaki *et al.*, 2015; Shi *et al.*, 2015), leading to cell death and the release of inflammatory cytosolic contents such as lactate dehydrogenase (LDH) and high mobility group box 1 (HMGB1). Consistent with its inhibitory effect on cell death, LOC14 inhibited the proteolytic cleavage of caspase-1 and GSDMD, and the release of LDH and HMGB1 in BMDMs stimulated with

LPS plus nigericin or LPS plus ATP (**Fig. 1E, Supplementary Fig. 1C**). In addition, IL-1β release, which accompanies caspase-1 and GSDMD activation, was abolished in these BMDMs following LOC14 treatment (**Fig. 1F, Supplementary Fig. 1D**). Expanding on the activators LPS plus nigericin or LPS plus ATP, which induce the activation of NLRP3 via a K^+ efflux-dependent manner, we tested LPS plus imiquimod, which induces the activation of NLRP3 independently of K^+ efflux (Gross *et al*, 2016). LOC14 inhibited K^+ efflux-independent NLRP3 inflammasome activation induced by LPS plus imiquimod (**Fig. 1G**).

To assess the role of LOC14 in human cells, we stimulated the human monocytic cell line THP1 with LPS plus nigericin in the presence or absence of LOC14. Treatment of LOC14 inhibited the proteolytic cleavage of caspase-1 and GSDMD (**Supplementary Fig. 1E**). Further, in primary human peripheral blood mononuclear cells (PBMCs) from healthy donors, LOC14 attenuated caspase-1 and GSDMD activation, and IL-1β release triggered by Pam3CSK4 plus nigericin (**Supplementary Fig. 1F, G**). Although LOC14 is also known as an allosteric inhibitor of protein disulfide isomerase A3 (PDIA3) (Kaplan *et al*, 2015), gene silencing of PDIA3 in BMDMs did not affect NLRP3 inflammasome activation, suggesting that the inhibitory effect of LOC14 on NLRP3 is independent of its action on PDIA3 (**Supplementary Fig. 2A–F**). These data collectively suggest that LOC14 is an inhibitor of the NLRP3 inflammasome in human and mouse cells.

LOC14 blocks non-canonical NLRP3 inflammasome activation

The NLRP3 inflammasome can also be activated by cytoplasmic LPS or infection with Gram-negative bacteria, through a pathway known as the non-canonical activation pathway owing to the requirement for the protease caspase-11 that binds LPS to initiate this process (Karki *et al*, 2020; Kayagaki *et al.*, 2015; Kayagaki *et al*, 2011; Shi *et al*, 2014). To determine whether LOC14 affects non-canonical NLRP3 inflammasome activation, we transfected LPS into BMDMs in the presence or absence of LOC14.

Caspase-1 activation and IL-1β release were reduced in LOC14-treated BMDMs, similar to CRID3-treated BMDMs (**Supplementary Fig. 3A, B**). In this case, LOC14 did not inhibit GSDMD cleavage (**Supplementary Fig. 3A**), which is due to caspase-11-dependent proteolytic cleavage of GSDMD that occurs prior to NLRP3 activation (Kayagaki *et al.*, 2011). Moreover, cell death analysis revealed similar kinetics of pyroptosis and the release of LDH in LPS-transfected BMDMs, in the presence or absence of LOC14 (**Supplementary Fig. 3A, C, D**). These data suggest that LOC14 does not inhibit caspase-11-dependent GSDMD processing and pyroptosis, but specifically blocks the activation of the NLRP3 inflammasome after caspase-11-mediated non-canonical activation.

LOC14 does not inhibit AIM2, NLRC4, NLRP1b and Pyrin inflammasomes

Next, we evaluated whether LOC14 functions against other inflammasomes. The DNA-sensing AIM2 inflammasome can be activated during infection with the bacterium *Francisella tularensis* subspecies *novicida* (*F. novicida*) or transfection of dsDNA poly(dA:dT) into the cytoplasm of mammalian cells (Fernandes-Alnemri *et al*, 2010; Rathinam *et al*, 2010). In the presence or absence of LOC14, we saw similar levels of caspase-1 and GSDMD proteolytic cleavage and cell death in BMDMs infected with *F. novicida* infection or transfected with poly(dA:dT), and similar induction of the transcription factor IRF1 in BMDMs infected with *F. novicida* infection or treated with IFN-β that were required to potentiate AIM2 inflammasome activation (**Fig. 2A–D, Supplementary Fig. 4A, B**) (Man *et al*, 2015; Man *et al*, 2016). These data suggest that LOC14 does not impair IRF1-dependent and IRF1-independent AIM2 inflammasome activation. The NLRP1b inflammasome is activated following the inhibition of cytosolic serine dipeptidases DPP8 and DPP9 (Okondo *et al*, 2018). However, LOC14 treatment did not impede the activation of caspase-1 and GSDMD or cell death following Val-boroPro stimulation (**Fig. 2E–G**). NLRC4 inflammasome is activated by bacterial flagellin, or rod and needle proteins of the Type III secretion

systems found in *Salmonella enterica* subspecies *enterica* serovar Typhimurium (*S.* Typhimurium) (Karki *et al*, 2018). LOC14 treatment did not affect caspase-1 and GSDMD activation and the rate of cell death in BMDMs following infection with *S.* Typhimurium (**Supplementary Fig. 4C, D**). Finally, Pyrin inflammasome activation occurs as a result of the inactivation of host Rho guanosine triphosphatases caused by infection with the bacterium *Clostridium difficile* (Xu *et al*, 2014). We observed that LOC14 treatment did not hinder Pyrin inflammasome activation induced by the supernatant of *Clostridium difficile* (**Supplementary Fig. 4E, F**). These results indicate that LOC14 does not interfere with the activation of the AIM2, NLRP1, NLRC4, and Pyrin inflammasomes.

LOC14 inhibits inflammasome oligomerization via binding to NLRP3

During inflammasome assembly, NLRP3 proteins form active oligomers in a disk-shape structure, where the C-terminal lobe of NEK7 nestles against both the LRR and NACHT of NLRP3, which is then required to form a larger complex with the inflammasome adaptor protein ASC (Sharif *et al.*, 2019; Xiao *et al*, 2023; Yu *et al*, 2024) Indeed, analysis using semi-denaturing detergent agarose-gel electrophoresis revealed that NLRP3 oligomerization induced by LPS plus ATP or LPS plus nigericin was impaired in BMDMs treated with LOC14 (**Fig. 3A**). Further, ASC oligomerization in BMDMs or the formation of ASC specks in human THP1 cells stimulated with LPS plus ATP or LPS plus nigericin were impaired in the presence of LOC14 (**Fig. 3B, Supplementary Fig. 5**). Taken together, these results indicate that LOC14 interferes with inflammasome complex assembly at an early stage by simultaneously impairing both NLRP3 oligomerization and subsequent ASC speck formation. Based on this observation, we hypothesized that LOC14 may exert its inhibitory effect by binding to NLRP3.

To test this possibility, we first used extra precision XP docking to investigate the interaction between LOC14 and human NLRP3 (**Supplementary Fig. 6A, B**). LOC14 bound to human NLRP3 with a similar affinity at –2.777 kcal/mol compared to

that between CRID3 and NLRP3 at –2.871 kcal/mol (**Fig. 3C**). Notably, in the presence of the kinase NEK7, LOC14 bound to human NLRP3 with an increased affinity at –5.012 kcal/mol (**Fig. 3C**). The presence of NEK7 did not increase the binding affinity between CRID3 and NLRP3 (**Fig. 3C**). We then used the Molecular Mechanics Generalized Born Surface Area method to assess the interaction between LOC14 and the NLRP3-NEK7 complex (Genheden & Ryde, 2015). The Gibbs free energy change (ΔG) value for LOC14 in the NLRP3-NEK7 complex was –48.92 kcal/mol (**Supplementary Fig. 6C**), indicating that NEK7 binding induces a conformation change on the surface architecture of NLRP3, generating an additional binding interface that enhances LOC14 affinity. To experimentally validate these *in silico* data, we used the drug affinity responsive target stability (DARTS) technique, which detects drug-protein interactions based on reduced protease susceptibility upon ligand binding(Lomenick *et al*, 2009). LOC14 protected endogenous NLRP3, but not ASC and caspase-1, from protease-mediated proteolysis in BMDMs (**Fig. 3D**). Further, in HEK293T cells expressing full-length human NLRP3 or mouse NLRP3, these proteins were resistant to protease-induced degradation (**Fig. 3E, Supplementary Fig. 7A**). However, full-length human NLRP6 expressed in HEK293T cells was not resistant to protease-induced degradation (**Supplementary Fig. 7B**). In addition, we used a NanoBRET probe to quantify the engagement between NLRP3 and LOC14 or CRID3 (Teske *et al*, 2024). In this assay, an NLRP3-Nluc protein is expressed in HEK293FT cells that binds to a fluorescent NanoBRET tracer. We found that the addition of either LOC14 or CRID3, but not the pan-caspase inhibitor qVD, to HEK293FT cells dose-dependently displaced the NanoBRET tracer from NLRP3 (**Fig. 3F**), suggesting that LOC14, similar to CRID3, can occupy NLRP3. Consistent with the high binding affinity of LOC14 to NLRP3, we found that LOC14 abolished the endogenous interaction between NLRP3 and NEK7 in THP1 cells (**Fig. 3G**). Together, these results demonstrate that LOC14

binds to NLRP3, disrupts the interaction between NLRP3 and NEK7, and thereby blocking inflammasome oligomerization at an early stage.

LOC14 binds to or near the LRR domain of NLRP3

To identify the specific domains of NLRP3 that bind LOC14, we expressed the LRR, NACHT, and PYD of NLRP3 in HEK293T cells and applied our DARTS assays (**Fig. 4A**). LOC14 protected the LRR, but not the NACHT or PYD, of NLRP3 against protease-induced degradation (**Fig. 4B, C**). Detailed analysis of stable molecular interactions between NLRP3, NEK7, and LOC14 revealed that the amino acid residue position R697 of NLRP3, located within the transition LRR domain (amino acid residue positions 640-742) (Hochheiser *et al*, 2022), formed a hydrogen bond with the carbonyl oxygen bridge found between the piperazine and cyclopropane chemical groups of LOC14. Further, the amino acid G696 of NLRP3 formed a hydrogen bond with the carbonyl oxygen of the benzisothiazolinone moiety of LOC14 (**Fig. 4D, E**). These data suggest that LOC14 binds to the transition LRR domain of NLRP3.

Given that CAPS patients carry gain-of-function mutations primarily in the NACHT domain of NLRP3, which causes hyperactive inflammasome assembly, we next asked whether LOC14 can suppress inflammasome hyperactivation driven by these NACHT domain mutations (Cosson *et al.*, 2024). To test this, we induced the expression of two well-characterized constitutively active NLRP3 mutants, D303H and K568N, in the human monocytic cell line U937 using doxycycline, leading to inflammasome-dependent cell death (Cosson *et al.*, 2024). Both mutants are non-responsive to CRID3 (Cosson *et al.*, 2024). LOC14 treatment dose-dependently inhibited cell death against both NLRP3 mutants **(Supplementary Fig. 8A, B).** Further, LOC14 blocked LPS-induced IL-1β in primary PBMCs from a patient with CAPS carrying the CRID3-responsive NLRP3 variant R490K **(Supplementary Fig. 8C).** These results suggest that LOC14 exerts its inhibitory effects by targeting near the LRR

domain, thereby suppressing hyperactivity caused by NLRP3 gain-of-function mutations.

The isothiazolinone moiety is the functional group inhibiting the NLRP3 inflammasome

LOC14 consists of two major chemical moieties: 1,2-Benzisothiazol-3(*2H*)-one (also known as BITO) and 1-(cyclopropylcarbonyl)piperazine-3(*2H*)-one (also known as PCP) (**Fig. 5A**), both of which are precursors for LOC14 synthesis (Kaplan *et al.*, 2015). We sought to determine the relative contributions of these chemical moieties in inhibiting NLRP3. BITO substantially reduced the cleavage of caspase-1 and GSDMD and inhibited cell death in BMDMs stimulated with LPS plus nigericin, similar to the levels achieved by LOC14 (**Fig. 5B, C**), whereas little inhibitory effects were observed for PCP (**Fig. 5B, C**).

From this inhibitory BITO moiety, we further removed the benzene ring within BITO to generate isothiazol-3(*2H*)-one (also known as ITO), and then systematically removed the carbonyl oxygen from ITO to generate isothiazole (also known as IT), then altered the position of the nitrogen atom IT to generate thiazole (also known as T), and finally replaced the sulfur atom in T with a nitrogen to generate imidazole (also known as I) (**Fig. 5D**). From these chemical subgroups, we saw ITO, but not IT, T and I inhibited NLRP3 inflammasome activation driven by LPS plus nigericin (**Fig. 5D–G**). Consistent with this, ITO and BITO attenuated NLRP3 inflammasome-induced cell death (**Supplementary Fig. 9A**). ITO also inhibited NLRP3 inflammasome activation in BMDMs infected with influenza A virus (**Supplementary Fig. 9B**). The IC_{50} values for BITO, ITO, LOC14, and CRID3 were 670 nM, 630 nM, 570 nM, and 450 nM, respectively (**Fig. 5H**). These results indicate that the carbonyl oxygen within the isothiazole ring of LOC14, BITO, and ITO is critical for NLRP3 inhibition. To test whether the isothiazolinone core structure remains essential when additional substituents are present, we next evaluated DCOIT (4,5-dichloro-2-n-octyl-4-isothiazoline-3-one) and

methylisothiazolinone (M-ITO). Both DCOIT and M-ITO exhibited a dose-dependent suppression of LPS plus ATP-induced cell death (**Supplementary Fig. 9C–F)**, supporting the functional importance of the isothiazolinone moiety in these chemical derivatives.

LOC14 inhibits priming of the NLRP3 inflammasome

NLRP3 inflammasome activation requires priming, which is regulated by both transcriptional upregulation of *Nlrp3* and *Il1b* expressions via Toll-like receptor (TLR) signaling and post-translational modifications (Bauernfeind *et al.*, 2009; Franchi *et al.*, 2009). To elucidate whether LOC14 also affects priming, BMDMs were treated with LOC14 during the LPS priming phase, or during the activation phase in the presence of nigericin or ATP (**Supplementary Fig. 10A**). LOC14 consistently abolished NLRP3 activation when used in the priming or activation phase (**Supplementary Fig. 10A–G**). In addition to the activation phase, LOC14 delayed the upregulation of NLRP3 and pro-IL-1β mRNA and protein expression in BMDMs treated with LPS alone (**Fig. 6A, Supplementary Fig. 11A**). These results suggest an inhibition of TLR4-NF-κB-dependent transcriptional upregulation of NLRP3 components. Furthermore, LOC14 delayed the kinetics of LPS-induced phosphorylation of priming signaling proteins IκBα, ERK, and JNK (**Fig. 6B**). In addition to TLR4-dependent priming by LPS, LOC14 suppressed the activation of pro-inflammatory signaling pathways and NLRP3 upregulation induced by the TLR2 activator Pam3 or TLR3 activator Poly I:C (**Fig. 6C, D, Supplementary Fig. 11A–C**). Importantly, ITO and BITO did not inhibit LPS-induced upregulation of NLRP3, whereas LOC14 slightly delayed this process. However, all compounds delayed induction of pro-IL-1β expression (**Supplementary Fig. 11D**). Furthermore, LOC14 caused a more pronounced inhibition of LPS-induced NF-κB and MAPK activation compared to BITO and ITO (**Supplementary Fig. 11E**). These findings imply that additional functional groups in LOC14 contribute to the inhibition of the inflammasome priming events.

LOC14 attenuates colitis, sepsis, and psoriasis

The NLRP3 inflammasome contributes to inflammatory disorders, including colitis, sepsis, and psoriasis (Sharma & Kanneganti, 2021; Swanson *et al.*, 2019). To evaluate the therapeutic potential of LOC14, we assessed the efficacy of LOC14 across three mouse models of inflammatory diseases. In dextran sulfate sodium (DSS)-induced colitis, WT mice given DSS were treated orally with LOC14 or vehicle once daily. Body weight changes were monitored for 9 days post-DSS administration. LOC14-treated mice exhibited less body weight loss and reduced colon shortening compared with vehicle-treated controls (**Fig. 7A, B, Supplementary Fig. 12A**). The levels of inflammasome-dependent cytokines IL-1β and IL-18 were significantly reduced in the colons of mice treated with LOC14 compared with mice treated with a vehicle control (**Fig. 7C**). Hematoxylin and eosin staining revealed diminished cellular infiltration and reduced colon damage in mice treated with LOC14 (**Fig. 7D**). Histologic parameters, including inflammation, ulceration, and hyperplasia, were markedly attenuated in the proximal, middle, and distal regions of the colon of mice treated with LOC14 (**Fig. 7D**).

In our second model of LPS-induced sepsis, mice that were orally administered with LOC14 had reduced circulating levels of IL-1β compared to mice treated with a vehicle control (**Supplementary Fig. 12B**). Finally, in a mouse model of psoriasis driven by topical application of the inflammation trigger imiquimod on the back skin of mice for 5 days, we tested the role of LOC14 in inhibiting inflammasome activation and inflammation. Mice treated daily with oral LOC14 showed reduced psoriasis severity defined by the PASI score, similar to that observed in mice treated with the anti-inflammatory compound methotrexate (**Fig. 8A, B**). Moreover, mice treated with LOC14 had reduced psoriatic lesions, such as erythema, scaling, and thickening of the skin, compared with mice treated with a vehicle control (**Fig. 8A, B**). We observed reduced cellular infiltration and epidermal thickness and cleavage of GSDMD in the skin of mice treated with LOC14 compared to mice treated with a vehicle control (**Fig.**

335 **8C–E**). These findings indicate that LOC14 exhibits anti-inflammatory physiological

336 effects across multiple models of inflammatory diseases.

Discussion

Inflammation is initiated by the innate immune system through a complex network of signaling pathways. Among these pathways, the NLRP3 inflammasome is a key player that has been implicated in a spectrum of inflammatory conditions, from autoinflammatory diseases to metabolic disorders and neurodegenerative conditions (Dubey *et al*, 2025; Karki *et al*, 2017; Sharma & Kanneganti, 2021; Swanson *et al.*, 2019). In this study, we identified isothiazolinone-containing drugs as potent inhibitors of NLRP3. The importance of our findings lies in the characterization of the mechanisms of action of LOC14 in inhibiting the NLRP3 inflammasome. LOC14 not only suppressed NLRP3 activation but also impeded the upregulation of NLRP3 inflammasome components. Unlike conventional NLRP3 inhibitors such as CRID3, which primarily target the ATPase activity of the NACHT domain (Coll *et al*, 2019; Tapia-Abellan *et al*, 2019), LOC14 acts by binding to or near the LRR domain of NLRP3. This binding disrupts critical interactions between NLRP3 and NEK7, thereby blocking subsequent protein complex assembly and oligomerization. Our data suggest that LOC14, via the carbonyl oxygen of its isothiazolinone moiety, forms a hydrogen bond with the NLRP3 residue G696 that is located at the NLRP3-NEK7 interface (Sharif *et al.*, 2019). This interaction may provide a molecular basis for the distinct inhibitory mechanism of LOC14. Importantly, this mechanism of action may enable LOC14 to inhibit both MCC950-responsive and MCC950-non-responsive NLRP3 mutants (Cosson *et al.*, 2024). This broad-spectrum efficacy highlights the therapeutic promise of LRR-targeting NLRP3 inhibitors in treating CAPS and other NLRP3-driven inflammatory disorders, especially those involving gain-of-function NLRP3 mutations resistant to current therapies.

LOC14 has a less inhibitory effect on NF-κB activation and NLRP3 upregulation compared to ERK activation and pro-IL-1β induction. This potential differential inhibition implies that NLRP3 upregulation is more reliant on NF-κB signaling, whereas

pro-IL-1β induction is more dependent on ERK activation. However, the inhibition of NLRP3 inflammasome activation by isothiazolinone-containing compounds at lower concentrations appears to be independent of any effect on inflammasome priming, as these compounds retained their suppressive activity without altering the priming step. The inhibitory effects of isothiazolinone on both priming and activation steps of NLRP3 may offer a broader applicability across different inflammatory diseases. Indeed, our *in vivo* results demonstrated the efficacy of LOC14 in three preclinical models of inflammatory diseases.

Importantly, LOC14 possesses favorable pharmacokinetic properties, including cell permeability, the ability to cross the blood-brain barrier, and oral bioavailability, with no reported toxicity (Kaplan *et al.*, 2015). The neuroprotective effects of LOC14 in a preclinical model of Huntington's disease are attributed to its role in inhibiting PDIA3 (Kaplan *et al.*, 2015; Zhou *et al*, 2018). It is conceivable that the PDIA3-independent, NLRP3-dependent effects of LOC14 might also contribute to the previously observed improvements in cognitive function following LOC14 treatment. Given the implication of inflammasomes in various neurological diseases, our findings potentially broaden the therapeutic application of isothiazolinone-containing drugs to neurological conditions. In conclusion, our findings report LOC14 and isothiazolinone compounds as selective inhibitors of the NLRP3 inflammasome with broad therapeutic effects for inflammatory diseases. Further clinical development of isothiazolinone derivatives as next-generation NLRP3 inhibitors will empower and advance anti-inflammatory therapeutics.

Materials and Methods

Mice

C57BL/6J (wild type) mice were purchased from Raonbio (Yongin, Korea). *Nlrp3*$^{-/-}$, *Aim2*$^{-/-}$, *Nlrc4*$^{-/-}$, and *Mefv*$^{-/-}$ mice were kindly provided by Dr. SangJoon Lee (Ulsan National Institute of Science and Technology) (Oh *et al*, 2023). Mice were housed and bred under protocols approved by the Seoul National University committee on the Use and Care of Animals. C57BL/6N mice were purchased from the Vital River Laboratory Animal Technology Co., Ltd (Beijing) and kept in a specific pathogen-free facility at the animal resource center at Shenzhen Bay Laboratory. Mice were maintained with a 12 h light/dark cycle and were fed standard chow. Both male and female age- and sex-matched 6- to 9-week old mice were used in this study. Animal studies were conducted under protocols approved by the Seoul National University committee and the Regional Ethics Committee for Animal Experiments at Shenzhen Bay Laboratory.

Cell culture

Primary bone marrow-derived macrophages (BMDMs) were obtained from the bone marrow of mice. Cells were cultured for 7 days in DMEM (Biowest, L0103-500) with 30% L929 conditioned media, 10% heat-inactivated fetal bovine serum (HI-FBS; Thermo Fischer Scientific, 16000044), 1% penicillin and streptomycin (Biowest, L0022-100), and 1% non-essential amino acids (Thermo Fisher Scientific, 11140-050). BMDMs were then seeded into DMEM media supplemented with 1% non-essential amino acids, 1% penicillin and streptomycin and 10% HI-FBS, at a density of 1×10^6 cells into 12-well plates and incubated at 37 °C overnight unless otherwise described. In the indicated experiments, DMEM media supplemented with 10% human serum (Biowest, S4190), 1% penicillin and streptomycin, and 1% non-essential amino acids were used during stimulation procedure. THP1-ASC-GFP cells were established by transducing

lentivirus expressing ASC-GFP and then selected via flow cytometry. The cells were grown in RPMI 1640 (Biowest, L0498) with 10% FBS.

Bacterial culture

F. novicida strain U112 was grown overnight under aerobic conditions at 37 °C in Tryptic Soy Broth (Formedium, TSB0110) supplemented with 0.2% L-cysteine (ThermoFisher Scientific, BP376-100). Bacteria were subcultured (1:10) for 4 h at 37 °C in fresh Trypticase Soy Broth supplemented with 0.2% L-cysteine. *Salmonella* Typhimurium strain SL1344 were inoculated into Luria-Bertani (LB) broth (Formedium, LMM0104) and incubated overnight under aerobic conditions at 37 °C. *S.* Typhimurium SL1344 were subcultured (1:10) for 4 h at 37 °C in fresh LB broth to generate bacteria grown to log phase. *C. difficile* ATCC 9689 (Korean Collection for Type Cultures, 5009) were streaked onto brain heart infusion agar (BD Biosciences, 211065) and incubated overnight at 37 °C in an anaerobic chamber. Single colonies were inoculated into tryptic-soy broth (Kisanbio, MB-T1054) with 5% sheep blood (Kisanbio, MB-S1876), 1% vitamin K1-hemin solution (Kisanbio, MB-V0761), 0.05% L-cysteine (ThermoFisher Scientific, BP376-100) at 37 °C anaerobically. The *C. difficile* supernatant was prepared by centrifugation to obtain the culture supernatant, followed by filtration of this supernatant through a 0.22 μm filter (Corning, 431219).

Influenza A virus culture

The influenza A virus (A/Puerto Rico/8/34, H1N1 [PR8]) was generated by reverse genetis as previously described (Zheng *et al*, 2015). Virus stocks were propagated by inoculation of seed virus into allantoic cavity of 9- to 11-day old embryonated chicken eggs. Virus titer was measured by plaque assay in MDCK cells. For IAV infection, BMDMs were infected at an MOI of 20 in DMEM plain media (Sigma, D6171). After

absorption for 2 h, cells were supplemented with 10% FBS and then incubated for the indicated time.

Cell stimulation

Seeded BMDMs were first gently washed with PBS before stimulation. For activation of the canonical NLRP3 inflammasome, cells were primed for 4 h with 100 ng/mL LPS (InvivoGen, tlrl-smlps) and were stimulated with 5 mM ATP (Roche, 10127531001) or 20 μM nigericin (Cayman, 11437) for indicated time with or without 5 μM LOC14 (Selleckchem, S0321), 1 μM CRID3 (Selleckchem, S7809), 5 μM 1,2-Benzisothiazol-3(*2H*)-one (Tokyo Chemical Industry, B3767), 5 μM 1-(cyclopropylcarbonyl)piperazine (Tokyo Chemical Industry, C3112), 5 μM Isothiazol-3(*2H*)-one (Tokyo Chemical Industry, I1172), 5 μM Isothiazol (Tokyo Chemical Industry, I0982), 5 μM Thiazole (Tokyo Chemical Industry, T0185), 5 μM Imidazole (Tokyo Chemical Industry, I001), 1 μM, 5 μM, 10 μM of 4,5-dichloro-2-n-octyl-4-isothiazoline-3-one (MedChemExpress, HY-W041308), and 1 μM, 5 μM, 10 μM of methylisothiazolinone (TargetMol, T19774). For NLRP3 inflammasome activation in human monocytes, THP1-ASC-GFP cells were plated in 24-well plates ($5x10^5$ cells per well) and treated with 100 ng/ml phorbol myristate acetate (Sigma-Aldrich, P1585) for 48 h for differentiation. Then cells were washed twice with PBS, followed by rest for another 24 h. Cells were first primed with 500 ng/ml LPS (Sigma-Aldrich, L2018) for 1 h and then treated with 10 μM nigericin plus 5 μM LOC14 (AbMole Bioscience, M9840), or nigericin plus 5 μM CRID3 (Sigma, 256373-96-c) for 45 min. For activation of potassium-independent NLRP3 inflammasome, cells were treated with 100 ng/ml LPS plus 20 μg/ml imiquimod (InvivoGen, tlrl-imqs). For transfection of DNA or LPS, each reaction consisted of 2 μg of poly(dA:dT) (InvivoGen, tlrl-patn) or 1 μg of LPS resuspended in PBS and mixed with 0.6 μL of Xfect polymer in Xfect reaction buffer (Clontech Laboratories Inc, 631318). After 10 min, DNA complexes were added to cells

that were preincubated in Opti-MEM (ThermoFisher Scientific, 31985070) for 1 h. For activation of the NLRP1 inflammasome, cells were treated with 50 μM Val-boroPro (Selleckchem, S8455) for indicated time. For mRNA expression and signaling, BMDMs were stimulated with 100 ng/ml LPS, 1 μg/ml Pam3CSK4 (InvivoGen, tlrl-pms), and 5 μg/ml PolyI:C HMW (InvivoGen, tlrl-pic) for indicated time. For bacterial infection, the following conditions were used: *F. novicida* at an MOI of 100 for 16 h of incubation (for activation of caspase-1 and GSDMD) and an MOI of 50 for 4, 12, or 24 h of incubation (for expression of IRF1); *S*. Typhimurium at an MOI of 0.1 for 3 h of incubation (for activation of caspase-1 and GSDMD). After 4 h of infection, bacteria were washed off with PBS and treated with 50 μg/ml gentamicin (ThermoFisher Scientific, 15750060).

Human blood was obtained with consent from donors in accordance with the Declaration of Helsinki, under protocols approved by the The Australian Capital Territory (ACT) Health Human Research Ethics Committee and The Australian National University Human Research Ethics Committee and under protocols ETH.1.16.011, 2022.ETH.00059, 2015/079, and H/2023/1429. Human peripheral blood mononuclear cells (PBMCs) were isolated from blood by density gradient centrifugation over Lymphoprep™ (07851, STEMCELL Technologies) and suspended at 1×10^7 cells/ml in RPMI-1640 supplemented with 10% FBS, 1% penicillin and streptomycin, and 1% l-Glutamine. PBMCs were seeded in antibiotic-free media at a concentration of 1×10^6 cells per well in 24-well plates. PBMCs were primed with Pam3CSK4 (InvivoGen, tlrl-pms) for 2.5 h, followed by treatment with either DMSO, 5 μM LOC14, or 10 μM CRID3 for 30 min. PBMCs were then stimulated with 10 μM nigericin (Sigma, N7143) for 1.5 h. PBMCs from a human patient with CAPS carrying an NLRP3 R490K mutation were seeded in antibiotic-free media at a concentration of 1×10^6 cells per well in 24-well plates. PBMCs were either left untreated or treated with DMSO, 10 μM LOC14, or 10 μM CRID3 for 30 min, followed by stimulation with *E. coli* LPS (Enzo Life Sciences, ALX-581-014-L002) for 6 h.

492

493 **Analysis of real-time cell death**

494 Real-time cell death assays were performed on an IncuCyte (Satorius, IncuCyte SX5).
495 BMDMs were seeded in 12-well plate and stimulated. Propidium iodide (Invitrogen,
496 P3566) were added at the time of stimulation for cell death analysis. Images (4 image
497 fields per well) were acquired every 15, 30 or 60 minutes depending on the expected
498 time frame for cell death at 37 °C and 5 % CO_2. Subsequent image analysis was
499 conducted using the software package supplied with the IncuCyte imager, the number
500 of propidium iodide-positive cells (PI^+ cells) present in each image were counted.
501 Representative images were selected at indicated time points.

502

503 **High-throughput screening**

504 A high-throughput screening (HTS) based on cell death induced by NLRP3
505 inflammasome activation was performed. Cell death triggered by LPS plus nigericin
506 was screened against a custom library (TargetMol), which included inhibitors targeting
507 more than 500 molecules across more than 100 signaling pathways, FDA-approved
508 drugs, clinical trial drugs, and natural products. BMDMs were seeded at a density of 2
509 $\times 10^5$ cells per well into 96-well plates and treated with each library compound at 5 μM.
510 The compounds were screened in duplicate, and real-time cell death assays were
511 performed using the IncuCyte system. Propidium iodide (PI) was added at the time of
512 stimulation for cell death analysis. Subsequent image analysis was conducted as
513 described in the previous section.

514

515 **Knockdown via small interfering RNAs (siRNAs)**

516 siRNAs specifically targeting *Pdia3* were chemically synthesized by Bionics, Korea. The
517 sequences of si-*Pdia3* were as follows: sense, 5’-GUGAAGGAGUACGAUGAUA-3’; and
518 antisense, 5’-UAUCAUCGUACUCCUUCAC-3’. A non-targeting siRNA was used as a

control. BMDMs were transfected with these oligos for 24 h using the Neon™ Transfection System (Invitrogen, MPK5000) according to the manufacturer's instructions. After transfection, the cells were stimulated with LPS and ATP or LPS and nigericin as previously described.

Immunoblot analysis

Immunoblotting was performed as described previously (Karki *et al*, 2021b). For caspase analysis, cells were lysed along with the supernatant using 50 µL caspase lysis buffer (containing 1 × protease inhibitors, 1 × phosphatase inhibitors, 10% NP-40 and 25 mM DTT) followed by the addition of 100 µL 4 × sample loading buffer (containing SDS and 2-mercaptoethanol). For analysis of LDHA and HMGB1, centrifuged (8000 rpm for 4min) supernatant 180 µL was combined with sample loading buffer 60 µL. For analysis of signaling proteins, supernatants were removed at the indicated time points, and cells were washed once with PBS, after which cells were lysed with RIPA buffer (containing 1 × phosphatase inhibitor, protease inhibitor, 1% NP-40, 0.5% Sodium deoxycholate) and sample loading buffer. Proteins were separated by electrophoresis through 8-12% polyacrylamide gels. Following electrophoretic transfer of proteins onto PVDF membranes (Millipore, IPVH00010), non-specific binding was blocked by incubation with 5% skim milk in TBST; then membranes were incubated at 4 ˚C for overnight with the following primary antibodies: caspase-1 (AdipoGen, AG-20B-0042, 1:1000), human cleaved caspase-1 (Cell Signaling, 4199, 1:1000), human caspase-1 (Cell Signaling, 2225, 1:1000), NEK7 (Abcam, ab133514, 1:1000), FLAG (Sigma, F1804, 1:5000), GSDMD (Abcam, ab209845, 1:1000), cleaved GSDMD (abcam, ab215203, 1:1000), LDHA (Proteintech, 19987-1-AP, 1:1000), ASC (AdipoGen, AG-25B-0006-C100, 1:1000), NLRP3/NALP3 (AdipoGen, AG-20B-0014-C100, 1:1000), HMGB1 (abcam, ab18256, 1:1000), SAPK/JNK (Cell Signaling, 9252, 1:1000), phospho-SAPK/JNK (Cell Signaling, 9251, 1:1000), IκB-alpha (Cell Signaling, 9242, 1:1000),

phospho-IκB-alpha (Cell Signaling, 2859, 1:1000), MAPK p44/42 (Cell Signaling, 9102, 1:1000), phospho-MAPK p44/42 (Cell Signaling, 9101, 1:1000), IRF1 (Cell Signaling, 8478, 1:1000), PDIA3 (Abclonal, A1085, 1:1000), IL-1β (Abclonal, A16288, 1:1000), GAPDH (CST, 5174S, 1:1000) and β-actin (Cell Signaling, 8457, 1:1000) antibodies. Membranes were then washed with TBST (10 min, 3 times) and incubated with appropriate secondary antibodies: HRP-conjugated anti-rabbit (Thermo Fisher Scientific, 31460, 1:5000) and HRP-conjugated anti-mouse (Cellnest, CNG004-0005, 1:5000) for 1 h, after which were washed with TBST (10 min, 4 times). Proteins were visualized by using Immobilon Forte Western HRP Substrate (Millipore, WBLUF0500), and the membranes were analyzed using Amersham ImageQuant 800 UV (Bae *et al*, 2025).

Real-time PCR (RT-PCR) analysis

Total RNA from cells was extracted with TRIzol reagent (Invitrogen, 15596026) following manufacturer's instructions. Isolated RNAs were reverse transcribed with M-MLV cDNA synthesis kit (Enzynomics, EZ006S) using the Applied Biosystems SimpliAmp thermal cycler (A24812) following manufacturers' instructions. Real-time qPCR was performed on QuantStudio 3 Real-Time PCR System by using TB green premix ex Taq (Takara, RR420) and ROX reference dye (Takara, AM21069A). Oligonucleotides used were as follows (Bionics): *Gapdh*: 5'-CGT CCC GTA GAC AAA ATG GT-3'(forward), 5'-TTG ATG GCA ACA ATC TCC AC-3' (reverse); and *Nlrp3*: 5'-TCA GAT TGC TGT GTG TGG GAC TGA-3' (forward), 5'-AGC TCA GAA CCA ATG CGA GAT CCT-3' (reverse).

Drug Affinity Responsive Target Stability (DARTS) assay

DARTS was carried out as described previously (Lomenick *et al.*, 2009). BMDMs were primed with LPS (50 ng/ml) for 3 h. HEK293T cells were harvested 24 h after

transfection with the indicated plasmids. Cells were lysed with NP-40 lysis buffer containing protease inhibitors. Lysates were centrifuged at 13,000 × g for 10 min at 4 °C and the protein concentration was measured with a BCA Protein Assay Kit (Beyotime Biotechnology). Lysates were incubated with LOC14 at the indicated concentrations overnight at 4 °C with rotation. Then, the protease pronase (200 ng of enzyme per reaction, AbMole Bioscience) was added to the lysates and incubated for 15 min at room temperature. The reaction was stopped by the addition of 4 × SDS loading buffer. The samples were then analyzed by immunoblotting.

NLRP3 Target Engagement assay

A NanoBRET® probe was used to quantify engagement between the NLRP3 and LOC14 or control inhibitors (Teske *et al.*, 2024). HEK293FT cells were transiently transfected with plasmids encoding NLRP3-Nluc fusion proteins. After 24 hours of transfection, HEK293FT cells were treated with serially diluted NLRP3 NanoBRET® tracer in the presence or absence of serially diluted LOC14 (AbMole Bioscience, M9840), MCC950 (Mathur *et al*, 2023), or qVD (Selleckchem, S7311). After 2 hours of equilibration, the NanoBRET® Target Engagement substrate solution and the inhibitor solution were added one after the other, and Bioluminescence Resonance Energy Transfer (BRET) was recorded on a VICTOR Nivo Plate Reader.

U937 expressing NLRP3-AID-associated mutant assays

NLRP3-deficient U937 cells reconstituted with the doxycycline-inducible NLRP3 D303H or K568N constitutively-active mutant have been previously described (Cosson *et al.*, 2024). 0.1×10^6 cells/ml were plated in Roswell Park Memorial Institute (RPMI) 1640 GlutaMaxTM-I supplemented with 1× penicillin and streptomycin and 10% FBS (Gibco). The next day, cells were treated the LOC14 (TA-T5534-5MG) at concentrations of 20, 10, or 5 µM in a final DMSO concentration of 0.2% (for 20 µM). 15 min later, cells

were treated with 2 μg/ml doxycycline (Sigma) before time-lapse imaging using a CQ1 high content screening microscope (Yokogawa) for 5 h. PI (1.25 μg/ml) and Hoechst (0.2 μg/ml) were added 1 h before imaging. 2 images per well were taken every 15 min for 5 h. Image analysis was performed as previously described (Cosson *et al.*, 2024).

NLRP3 oligomerization assay

NLRP3 oligomerization was determined by using semi-denaturing detergent agarose gel electrophoresis (SDD-AGE). BMDMs lysate was mixed with SDD-AGE loading dye (0.5% TAE, 5% glycerol, 2% sarcosyl, 0.1mg/ml bromophenol blue, and protease inhibitor) without boiling. Capillary transfer method was used to transfer the proteins to PVDF membrane as described previously (Hanna-Addams & Wang, 2018). Input lysate was boiled in 4 × sample loading buffer (containing SDS and 2-mercaptoethanol) and run for SDS-PAGE.

ASC oligomerization assay

After stimulation with ATP or nigericin, BMDMs were rinsed in ice-cold PBS and then lysed with NP-40 buffer (20 mM HEPES-KOH pH 7.5, 10 mM KCL, 1 mM EGTA, 1 mM EDTA, 320 mM sucrose, protease inhibitor) and incubated 10 min on ice. Collected lysates were passed through a 21-gauge needle at least 10 times to further disrupt the cells and then incubated on ice for 5 min. 30 μl of cell lysate was used for input. The remaining lysates were centrifuged at 3400 × g for 15 min at 4 °C. After removing the supernatants, the pellets were washed once with PBS and were centrifuged at 3400 x g for 15 min at 4 °C. The pellets were resuspended in 500 μl PBS containing 2 mM suberic acid bis (Sigma, S1885). The samples were incubated at RT for an hour for cross-linking and centrifuged at 10,000 × g for 15 minutes at 4 °C. The supernatants were aspirated, and the pellets were resuspended with 35 μl of 2 x loading dye. Both

input and cross-linked samples were incubated at 95 °C for 5 min and analyzed by immunoblot (Zangiabadi *et al*, 2022).

ASC specks formation

After stimulation with LPS and nigericin, THP1-ASC-GFP cells were rinsed with ice-cold PBS. The cells were then fixed with 4% paraformaldehyde for 10 min at room temperature, followed by three washes with PBS. ASC specks were visualized by immunofluorescence microscopy.

Co-immunoprecipitation assay

THP1-ASC-GFP cells (1×10^7 cells) were plated in 10 cm dishes and treated for 45 min as indicated. Following treatment, the cells were collected and washed once with ice-cold PBS. Cells were then lysed using NP-40 lysis buffer containing protease inhibitors. The cell lysates were centrifuged at 13,000 × g for 10 min at 4 °C. The supernatant was incubated overnight with 1 µg anti-NLRP3 (AG-20B-0014, Adipogen) or mouse IgG (Cell Signaling, 5415) antibody at 4 °C with rotation. After overnight incubation, protein A/G Agarose Resin (Yeason, 36403ES) was added to the lysates and further incubated for 1 h at 4 °C. The agarose resin was then washed 5 times with NP-40 lysis buffer. The samples were mixed with 2 × SDS loading buffer and boiled at 100 °C for 5 min.

Mouse models of inflammatory diseases

LPS-induced systemic inflammation: 7- to 8-week-old female WT mice were injected intraperitoneally with 20 mg/kg body weight of LPS (Sigma, L2630) (Karki *et al*, 2021a). Thirty minutes prior to the LPS injection, mice were administered intraperitoneally with either 200 µL of vehicle (10% DMSO in PBS, n = 10), or LOC14

(10 mg/kg body weight, n = 10). After 4 h, serum was collected and IL-1β levels were measured by ELISA.

DSS-induced colitis: Colitis was induced in 7- to 8-week-old female WT mice using dextran sodium sulfate (DSS) as described previously (Karki *et al*, 2016). Mice were randomly divided into four groups: Normal (n = 7), DSS (n= 9), DSS + 5 mg/kg LOC14 (n= 9), and DSS + 10 mg/kg LOC14 (n= 9). LOC14 was administered via intraperitoneal injection daily for 9 days. Both the normal and DSS-only (Yeason, 60316ES25) groups received the same volume of DMSO. Body weight was monitored daily. On day 9, mice were sacrificed, colon length was measured, serum was collected, and colons were submitted for histological analysis.

IMQ-induced skin inflammation (psoriasis): 7- to 8-week-old female WT mice were randomly divided into four groups: Normal (Vaseline, n = 10), Imiquimod (IMQ, n = 9), IMQ + Isothiazol3(*2H*)-one (ITO, n = 8), and IMQ + methotrexate (MTX, n = 7). To induce psoriasis-like skin inflammation, mice were topically applied Aldara, a cream containing 5% IMQ cream, on the shaved back skin (62.5 mg per mouse, Dong-A Science Technology) for 6 days. The normal group received the same amount of Vaseline. Starting one day after IMQ application, mice were orally administered ITO (10 mg/kg) or MTX (1 mg/kg, Yuhan Corporation) daily. To score the severity of inflammation of the back skin, an objective scoring system was used based on the clinical Psoriasis Area and Severity Index (PASI) (van der Fits *et al*, 2009). Erythema, scaling, and thickening were scored independently on a scale from 0 to 4: 0, none; 1, slight; 2, moderate; 3, marked; 4, very marked. The cumulative score (erythema plus scaling plus thickening) served as a measure of the severity of inflammation (scale 0–12). Mice were sacrificed on day 7, and skin tissues were submitted for histological analysis or homogenized in RIPA lysis buffer.

679

680 **Histological analysis**

681 The back skin and colon were fixed in 4% formaldehyde (Cellnest, CNP015-1000).
682 Tissue processing and H&E staining for skin and colons were performed by DKKorea
683 and Wuhan Servicebio Technology Laboratory, respectively. The stained sections were
684 digitized using a whole slide imaging system (Olympus VS200) at 20 x objective
685 magnification with a consistent scanning setting across the same set of experiments.

686

687 **Cytokine analysis**

688 Cytokines were measured by performing ELISA for mouse IL-18 (Invitrogen, BMS618-
689 3), mouse IL-1β (Invitrogen, 88-7013-88), and human IL-1β (ThermoFisher, BMS224-
690 2TEN) according to the manufacturers' instructions.

691

692 **Docking analysis**

693 *Preparation of receptor and ligands*: The structure of NLRP3-NEK7 complex was
694 retrieved from the Protein Databank (PDB) with the ID 6NPY (Sharif *et al.*, 2019). The
695 Protein Preparation Wizard tool was utilized to assign hydrogen atoms, and charges.
696 The OPLS_2005 force field was used to optimize ionization and tautomeric states
697 (Jorgensen *et al*, 1996). The 3D structure of LOC14 (PubChem ID: 9117962) was
698 downloaded as a structure data file (SDF). LigPrep (Schrödinger Release 2024-2) was
699 applied to verify chiral centers. The NLRP3 protein consists of 2 chains. Chain A
700 includes the NACHT, LRR, and PYD domains, while B comprises the Serine/threonine-
701 protein kinase NEK7. To investigate the interaction between NLRP3 and NEK7, the
702 Receptor Grid Generation tool was used to define the active site. The active site of
703 NLRP3 included P134, E135, A614, K615, A616, K617, K618, L619, Q620, I621, Q622,
704 P623, S624, Q625, E627, L628, F629, Y630, C631, L632, Q636, E637, E638, D639,
705 A644, M645, K694, E695, G696, R697, H698, L699, N720 residues. For NEK7, the

active site included residues D261, H262, Y263, S264, C298, and T299. The receptor-ligand docking study was conducted using the Glide (grid-based ligand docking with extra precision (XP)) tool from the Schrödinger molecular modeling package (Halgren *et al*, 2004).

Molecular dynamic simulation: The Molecular Dynamics (MD) simulation of the NLRP3-NEK7-LOC14 complex was conducted using the Desmond package (Schrödinger Release 2024-2) for a duration of 1000 ns. The complex was prepared using a protein preparation wizard, which involved inserting hydrogen atoms, removing water molecules, assigning bond orders, and completing missing side chains and loops. Hydrogen-bond assignments were optimized at a pH of 7.0, and water orientations were sampled. Energy minimization of the protein-ligand complexes was performed using the OPLS-2005 force field (Price & Brooks, 2004).

The system was assembled using the TIP3P solvent model, creating a 10 Å buffer around the complex in an orthorhombic simulation box. Na^+ ions and Cl^- counter ions were added to achieve a physiological salt concentration of 0.15 M and to neutralize the system. The MD simulation was run under an NPT (constant Number of particles, Pressure, and Temperature) ensemble at a temperature of 300 K and a pressure of 1.013 bar (Patel *et al*, 2023). Surface tension was calculated using the Smooth Particle Mesh Ewald (PME) method (Essmann *et al*, 1995) to account for long-range electrostatic interactions, with the RESPA integrator used for potential energy calculations (Wang *et al*, 2006).

The simulation was performed for 1000 ns, capturing 1000 frames throughout the duration. The resulting trajectories were analyzed using the Simulation Interaction Diagram wizard to calculate Root Mean Square Deviation (RMSD) and Root Mean Square Fluctuation (RMSF) values (Zhang & Lazim, 2017). Protein-ligand contact patterns and the duration of interactions for key amino acid residues were assessed

over the simulation period. The MD simulation approach was used to validate the docking postures and the interactions predicted by both ligands with the NLRP3 protein.

Binding free energy calculations: The Gibb's free energy change was performed using the Molecular Mechanics Generalized Born Surface Area (MM-GBSA) method to analyze the interaction between the LOC14 and NLRP3-NEK7 protein complex (Hou *et al*, 2011; Massova & Kollman, 2000). The initial step involved conducting MD stimulation to generate an output file containing the trajectories and conformations of the protein-ligand complex. The MD stimulation output file was input into Schrödinger Maestro's Prime wizard for further optimization. The optimized structures were used to calculate the binding free energy using the OPLS-2005 force field. The change in free energy upon binding (ΔG) was determined by the following equation:

$$\Delta G_{Bind} = \Delta E_{MM} + \Delta G_{Solv} + \Delta G_{SA}$$

Where:

$\Delta G_{Bind:}$ Molar Gibbs free energy change associated with the binding of the receptor and ligand in solution.

$\Delta E_{MM:}$ Difference in the molecular mechanics energy between the minimal energy states of the protein-ligand complex.

$\Delta G_{Solv:}$ Total solvation energy, comprising the solvation energies of the protein and ligand and the change in GBSA solvation energy.

$\Delta G_{SA:}$ Difference in surface area energies between the free and bound states.

Statistical analysis

GraphPad Prism 9.0 software was used for data analysis. The data are presented as the mean ± SEM. Statistical significance was determined using a t test (two-tailed) or one-way ANOVA and two-way ANOVA with multiple comparisons for multiple groups. P

values less than 0.05 were considered statistically significant and are indicated as *P < 0.05, **P < 0.01, ***P < 0.001, and ****P < 0.0001.

Acknowledgments

We thank all the members of the Karki laboratory for their comments and suggestions during the development of this manuscript. We acknowledge the contribution of SFR Biosciences (Université Claude Bernard Lyon 1, CNRS UAR3444, Inserm US8, ENS de Lyon) and the help of the staff of LyMIC-PLATIM, especially Elodie Chatre, for assistance with HCS microscopy. We acknowledge Ann-Maree Padarin (The Australian National University) for assistance with obtaining human blood.

This work was supported by the Creative-Pioneering Researchers Program through Seoul National University (3344-20240032 to RK), National Research Foundation of Korea (NRF) grant funded by the Korea government (MSIT) (RS-2023-00251395 to RK), National Research Foundation of Korea (NRF) grant funded by the Korea government (MSIT) (RS-2025-00554099 to RK), Bio&Medical Technology Development Program of the National Research Foundation (NRF) funded by the Korea government (MSIT) (RS-2024-00440738 to RK), BK21 Research Fellowship from the Ministry of Education, Science and Technology, Republic of Korea (to RK), and CSL Centenary Fellowship (to SMM).

Author contributions

HW, YJ, and RK conceived and designed the study. HW, YJ, SK, WK, RM, CNP, MZ, MK, CN, SHJ, AN, BFP, SMM, and RK designed and performed the experiments. SHJ, MZ, SMM, and RK provided reagents and funding. HW, YJ, SMM, and RK wrote the manuscript. HW, YJ, SK, WK, FZ, RM, CNP, MK, MZ, SMM, and RK revised the manuscript. RK supervised the study and provided funding. All authors read and approved the manuscript.

Conflict of Interests

HW, YJ, and RK reported a provisional patent application (KR 10-2024-0124191) on LOC14 and isothiazolinone, filed by Seoul National University; those authors are listed as inventors. No other disclosures were reported.

Additional Information

The datasets generated and analyzed during the current study are contained within the manuscript and the accompanying extended data figures. Source data are provided with this paper. Correspondence and requests for materials should be addressed to MZ, SMM, and RK.

References

Aganna E, Martinon F, Hawkins PN, Ross JB, Swan DC, Booth DR, Lachmann HJ, Bybee A, Gaudet R, Woo P *et al* (2002) Association of mutations in the NALP3/CIAS1/PYPAF1 gene with a broad phenotype including recurrent fever, cold sensitivity, sensorineural deafness, and AA amyloidosis. *Arthritis Rheum* 46: 2445-2452

Anand PK (2025) From fat to fire: The lipid-inflammasome connection. *Immunol Rev* 329: e13403

Bae H, Moon S, Chang M, Zhang F, Jang Y, Kim W, Kim S, Fu M, Lim J, Park S *et al* (2025) Ferroptosis-activating metabolite acrolein antagonizes necroptosis and anti-cancer therapeutics. *Nat Commun* 16: 4919

Bauernfeind FG, Horvath G, Stutz A, Alnemri ES, MacDonald K, Speert D, Fernandes-Alnemri T, Wu J, Monks BG, Fitzgerald KA *et al* (2009) Cutting edge: NF-kappaB activating pattern recognition and cytokine receptors license NLRP3 inflammasome activation by regulating NLRP3 expression. *J Immunol* 183: 787-791

Coll RC, Hill JR, Day CJ, Zamoshnikova A, Boucher D, Massey NL, Chitty JL, Fraser JA, Jennings MP, Robertson AAB *et al* (2019) MCC950 directly targets the NLRP3 ATP-hydrolysis motif for inflammasome inhibition. *Nat Chem Biol* 15: 556-559

Coll RC, Robertson AA, Chae JJ, Higgins SC, Munoz-Planillo R, Inserra MC, Vetter I, Dungan LS, Monks BG, Stutz A *et al* (2015) A small-molecule inhibitor of the NLRP3 inflammasome for the treatment of inflammatory diseases. *Nat Med* 21: 248-255

Coll RC, Schroder K (2025) Inflammasome components as new therapeutic targets in inflammatory disease. *Nat Rev Immunol* 25: 22-41

Cosson C, Riou R, Patoli D, Niu T, Rey A, Groslambert M, De Rosny C, Chatre E, Allatif O, Henry T *et al* (2024) Functional diversity of NLRP3 gain-of-function mutants associated with CAPS autoinflammation. *J Exp Med* 221

Dubey SR, Turnbull C, Pandey A, Zhao A, Kurera M, Al-Zidan R, Shen C, Gautam M, Mahajan S, Jadhav PS *et al* (2025) Molecular mechanisms and regulation of inflammasome activation and signaling: sensing of pathogens and damage molecular patterns. *Cell Mol Immunol*

Duewell P, Kono H, Rayner KJ, Sirois CM, Vladimer G, Bauernfeind FG, Abela GS, Franchi L, Nunez G, Schnurr M *et al* (2010) NLRP3 inflammasomes are required for atherogenesis and activated by cholesterol crystals. *Nature* 464: 1357-1361

Essmann U, Perera L, Berkowitz ML, Darden T, Lee H, Pedersen LG (1995) A Smooth Particle Mesh Ewald Method. *J Chem Phys* 103: 8577-8593

Feldmann J, Prieur AM, Quartier P, Berquin P, Certain S, Cortis E, Teillac-Hamel D, Fischer A, de Saint Basile G (2002) Chronic infantile neurological cutaneous and articular syndrome is caused by mutations in CIAS1, a gene highly expressed in polymorphonuclear cells and chondrocytes. *Am J Hum Genet* 71: 198-203

Feng S, Wierzbowski MC, Hrovat-Schaale K, Dumortier A, Zhang Y, Zyulina M, Baker PJ, Reygaerts T, Steiner A, De Nardo D *et al* (2025) Mechanisms of NLRP3 activation and inhibition elucidated by functional analysis of disease-associated variants. *Nat Immunol* 26: 511-523

Fernandes-Alnemri T, Yu JW, Juliana C, Solorzano L, Kang S, Wu J, Datta P, McCormick M, Huang L, McDermott E *et al* (2010) The AIM2 inflammasome is critical for innate immunity to Francisella tularensis. *Nat Immunol* 11: 385-393

Franchi L, Eigenbrod T, Nunez G (2009) Cutting edge: TNF-alpha mediates sensitization to ATP and silica via the NLRP3 inflammasome in the absence of microbial stimulation. *J Immunol* 183: 792-796

Genheden S, Ryde U (2015) The MM/PBSA and MM/GBSA methods to estimate ligand-binding affinities. *Expert Opin Drug Discov* 10: 449-461

Gross CJ, Mishra R, Schneider KS, Medard G, Wettmarshausen J, Dittlein DC, Shi H, Gorka O, Koenig PA, Fromm S *et al* (2016) K(+) Efflux-Independent NLRP3

Inflammasome Activation by Small Molecules Targeting Mitochondria. *Immunity* 45: 761-773

Gurung P (2025) Innate Immune Sensors in Health and Disease. *Immunol Rev* 330: e70008

Halgren TA, Murphy RB, Friesner RA, Beard HS, Frye LL, Pollard WT, Banks JL (2004) Glide: A new approach for rapid, accurate docking and scoring. 2. Enrichment factors in database screening. *J Med Chem* 47: 1750-1759

Hanna-Addams S, Wang Z (2018) Use of Two Dimensional Semi-denaturing Detergent Agarose Gel Electrophoresis to Confirm Size Heterogeneity of Amyloid or Amyloid-like Fibers. *J Vis Exp*

He Y, Zeng MY, Yang D, Motro B, Nunez G (2016) NEK7 is an essential mediator of NLRP3 activation downstream of potassium efflux. *Nature* 530: 354-357

Heneka MT, Kummer MP, Stutz A, Delekate A, Schwartz S, Vieira-Saecker A, Griep A, Axt D, Remus A, Tzeng TC *et al* (2013) NLRP3 is activated in Alzheimer's disease and contributes to pathology in APP/PS1 mice. *Nature* 493: 674-678

Hochheiser IV, Pilsl M, Hagelueken G, Moecking J, Marleaux M, Brinkschulte R, Latz E, Engel C, Geyer M (2022) Structure of the NLRP3 decamer bound to the cytokine release inhibitor CRID3. *Nature* 604: 184-189

Hoffman HM, Mueller JL, Broide DH, Wanderer AA, Kolodner RD (2001) Mutation of a new gene encoding a putative pyrin-like protein causes familial cold autoinflammatory syndrome and Muckle-Wells syndrome. *Nat Genet* 29: 301-305

Hollis A, Lukens JR (2025) Role of inflammasomes and neuroinflammation in epilepsy. *Immunol Rev* 329: e13421

Hou TJ, Wang JM, Li YY, Wang W (2011) Assessing the Performance of the MM/PBSA and MM/GBSA Methods. 1. The Accuracy of Binding Free Energy Calculations Based on Molecular Dynamics Simulations. *J Chem Inf Model* 51: 69-82

Jorgensen WL, Maxwell DS, TiradoRives J (1996) Development and testing of the OPLS all-atom force field on conformational energetics and properties of organic liquids. *J Am Chem Soc* 118: 11225-11236

Kaplan A, Gaschler MM, Dunn DE, Colligan R, Brown LM, Palmer AG, 3rd, Lo DC, Stockwell BR (2015) Small molecule-induced oxidation of protein disulfide isomerase is neuroprotective. *Proc Natl Acad Sci U S A* 112: E2245-2252

Karki R, Kanneganti TD (2019) Diverging inflammasome signals in tumorigenesis and potential targeting. *Nat Rev Cancer* 19: 197-214

Karki R, Kanneganti TD (2021) The 'cytokine storm': molecular mechanisms and therapeutic prospects. *Trends Immunol* 42: 681-705

Karki R, Lee E, Place D, Samir P, Mavuluri J, Sharma BR, Balakrishnan A, Malireddi RKS, Geiger R, Zhu Q *et al* (2018) IRF8 Regulates Transcription of Naips for NLRC4 Inflammasome Activation. *Cell* 173: 920-933 e913

Karki R, Lee E, Sharma BR, Banoth B, Kanneganti TD (2020) IRF8 Regulates Gram-Negative Bacteria-Mediated NLRP3 Inflammasome Activation and Cell Death. *J Immunol* 204: 2514-2522

Karki R, Man SM, Kanneganti TD (2017) Inflammasomes and Cancer. *Cancer Immunol Res* 5: 94-99

Karki R, Man SM, Malireddi RKS, Kesavardhana S, Zhu Q, Burton AR, Sharma BR, Qi X, Pelletier S, Vogel P *et al* (2016) NLRC3 is an inhibitory sensor of PI3K-mTOR pathways in cancer. *Nature* 540: 583-587

Karki R, Sharma BR, Tuladhar S, Williams EP, Zalduondo L, Samir P, Zheng M, Sundaram B, Banoth B, Malireddi RKS *et al* (2021a) Synergism of TNF-alpha and IFN-gamma Triggers Inflammatory Cell Death, Tissue Damage, and Mortality in SARS-CoV-2 Infection and Cytokine Shock Syndromes. *Cell* 184: 149-168 e117

Karki R, Sundaram B, Sharma BR, Lee S, Malireddi RKS, Nguyen LN, Christgen S, Zheng M, Wang Y, Samir P *et al* (2021b) ADAR1 restricts ZBP1-mediated immune response and PANoptosis to promote tumorigenesis. *Cell Rep* 37: 109858

Kayagaki N, Stowe IB, Lee BL, O'Rourke K, Anderson K, Warming S, Cuellar T, Haley B, Roose-Girma M, Phung QT *et al* (2015) Caspase-11 cleaves gasdermin D for non-canonical inflammasome signalling. *Nature* 526: 666-671

Kayagaki N, Warming S, Lamkanfi M, Vande Walle L, Louie S, Dong J, Newton K, Qu Y, Liu J, Heldens S *et al* (2011) Non-canonical inflammasome activation targets caspase-11. *Nature* 479: 117-121

Kim JE, Lee JY, Kang MJ, Jeong YJ, Choi JA, Oh SM, Lee KB, Park JH (2015) Withaferin A Inhibits Helicobacter pylori-induced Production of IL-1beta in Dendritic Cells by Regulating NF-kappaB and NLRP3 Inflammasome Activation. *Immune Netw* 15: 269-277

Kim W, Kim S, Woo H, Jojare RA, Mall R, Nicotra A, Py BF, Ngo C, Man SM, Patel CN *et al* (2025) A potent NLRP3 inhibitor effective against both MCC950-sensitive and -resistant inflammation. *Cell Chem Biol* 32: 1125-1139 e1127

Lamkanfi M, Dixit VM (2014) Mechanisms and functions of inflammasomes. *Cell* 157: 1013-1022

Li L, Xu T, Qi X (2025) Balanced regulation of ROS production and inflammasome activation in preventing early development of colorectal cancer. *Immunol Rev* 329: e13417

Lomenick B, Hao R, Jonai N, Chin RM, Aghajan M, Warburton S, Wang J, Wu RP, Gomez F, Loo JA *et al* (2009) Target identification using drug affinity responsive target stability (DARTS). *Proc Natl Acad Sci U S A* 106: 21984-21989

Man SM, Kanneganti TD (2024) Innate immune sensing of cell death in disease and therapeutics. *Nat Cell Biol* 26: 1420-1433

Man SM, Karki R, Malireddi RK, Neale G, Vogel P, Yamamoto M, Lamkanfi M, Kanneganti TD (2015) The transcription factor IRF1 and guanylate-binding proteins target activation of the AIM2 inflammasome by Francisella infection. *Nat Immunol* 16: 467-475

Man SM, Karki R, Sasai M, Place DE, Kesavardhana S, Temirov J, Frase S, Zhu Q, Malireddi RKS, Kuriakose T *et al* (2016) IRGB10 Liberates Bacterial Ligands for Sensing by the AIM2 and Caspase-11-NLRP3 Inflammasomes. *Cell* 167: 382-396 e317

Mangan MSJ, Olhava EJ, Roush WR, Seidel HM, Glick GD, Latz E (2018) Targeting the NLRP3 inflammasome in inflammatory diseases. *Nat Rev Drug Discov* 17: 588-606

Martinon F, Petrilli V, Mayor A, Tardivel A, Tschopp J (2006) Gout-associated uric acid crystals activate the NALP3 inflammasome. *Nature* 440: 237-241

Massova I, Kollman PA (2000) Combined molecular mechanical and continuum solvent approach (MM-PBSA/GBSA) to predict ligand binding. *Perspect Drug Discov* 18: 113-135

Mathur A, Kay C, Xue Y, Pandey A, Lee J, Jing W, Enosi Tuipulotu D, Lo Pilato J, Feng S, Ngo C *et al* (2023) *Clostridium perfringens* virulence factors are nonredundant activators of the NLRP3 inflammasome. *EMBO Rep* 24: e54600

Oh S, Lee J, Oh J, Yu G, Ryu H, Kim D, Lee S (2023) Integrated NLRP3, AIM2, NLRC4, Pyrin inflammasome activation and assembly drive PANoptosis. *Cell Mol Immunol* 20: 1513-1526

Okondo MC, Rao SD, Taabazuing CY, Chui AJ, Poplawski SE, Johnson DC, Bachovchin DA (2018) Inhibition of Dpp8/9 Activates the Nlrp1b Inflammasome. *Cell Chem Biol* 25: 262-267 e265

Pandey A, Li Z, Gautam M, Ghosh A, Man SM (2025) Molecular mechanisms of emerging inflammasome complexes and their activation and signaling in inflammation and pyroptosis. *Immunol Rev* 329: e13406

Patel CN, Mall R, Bensmail H (2023) AI-driven drug repurposing and binding pose meta dynamics identifies novel targets for monkeypox virus. *J Infect Public Heal* 16: 799-807

Price DJ, Brooks CL (2004) A modified TIP3P water potential for simulation with Ewald summation. *J Chem Phys* 121: 10096-10103

Rathinam VA, Jiang Z, Waggoner SN, Sharma S, Cole LE, Waggoner L, Vanaja SK, Monks BG, Ganesan S, Latz E *et al* (2010) The AIM2 inflammasome is essential for host defense against cytosolic bacteria and DNA viruses. *Nat Immunol* 11: 395-402

Schmid-Burgk JL, Chauhan D, Schmidt T, Ebert TS, Reinhardt J, Endl E, Hornung V (2016) A Genome-wide CRISPR (Clustered Regularly Interspaced Short Palindromic Repeats) Screen Identifies NEK7 as an Essential Component of NLRP3 Inflammasome Activation. *J Biol Chem* 291: 103-109

Sharif H, Wang L, Wang WL, Magupalli VG, Andreeva L, Qiao Q, Hauenstein AV, Wu Z, Nunez G, Mao Y *et al* (2019) Structural mechanism for NEK7-licensed activation of NLRP3 inflammasome. *Nature* 570: 338-343

Sharma BR, Kanneganti TD (2021) NLRP3 inflammasome in cancer and metabolic diseases. *Nat Immunol* 22: 550-559

Shi HX, Wang Y, Li XH, Zhan XM, Tang M, Fina M, Su LJ, Pratt D, Bu CH, Hildebrand S *et al* (2016) NLRP3 activation and mitosis are mutually exclusive events coordinated by NEK7, a new inflammasome component. *Nat Immunol* 17: 250-258

Shi J, Zhao Y, Wang K, Shi X, Wang Y, Huang H, Zhuang Y, Cai T, Wang F, Shao F (2015) Cleavage of GSDMD by inflammatory caspases determines pyroptotic cell death. *Nature* 526: 660-665

Shi J, Zhao Y, Wang Y, Gao W, Ding J, Li P, Hu L, Shao F (2014) Inflammatory caspases are innate immune receptors for intracellular LPS. *Nature* 514: 187-192

Swanson KV, Deng M, Ting JP (2019) The NLRP3 inflammasome: molecular activation and regulation to therapeutics. *Nat Rev Immunol* 19: 477-489

Tapia-Abellan A, Angosto-Bazarra D, Martinez-Banaclocha H, de Torre-Minguela C, Ceron-Carrasco JP, Perez-Sanchez H, Arostegui JI, Pelegrin P (2019) MCC950 closes the active conformation of NLRP3 to an inactive state. *Nat Chem Biol* 15: 560-564

Teske KA, Corona C, Wilkinson J, Mamott D, Good DA, Zambrano D, Lazar DF, Cali JJ, Robers MB, O'Brien MA (2024) Interrogating direct NLRP3 engagement and functional inflammasome inhibition using cellular assays. *Cell Chem Biol* 31: 349-360 e346

van der Fits L, Mourits S, Voerman JS, Kant M, Boon L, Laman JD, Cornelissen F, Mus AM, Florencia E, Prens EP *et al* (2009) Imiquimod-induced psoriasis-like skin inflammation in mice is mediated via the IL-23/IL-17 axis. *J Immunol* 182: 5836-5845

Vande Walle L, Lamkanfi M (2024) Drugging the NLRP3 inflammasome: from signalling mechanisms to therapeutic targets. *Nat Rev Drug Discov* 23: 43-66

Vande Walle L, Stowe IB, Sacha P, Lee BL, Demon D, Fossoul A, Van Hauwermeiren F, Saavedra PHV, Simon P, Subrt V *et al* (2019) MCC950/CRID3 potently targets the NACHT domain of wild-type NLRP3 but not disease-associated mutants for inflammasome inhibition. *PLoS Biol* 17: e3000354

Wang JM, Hou TJ, Xu XJ (2006) Recent Advances in Free Energy Calculations with a Combination of Molecular Mechanics and Continuum Models. *Curr Comput-Aid Drug* 2: 287-306

Wannamaker W, Davies R, Namchuk M, Pollard J, Ford P, Ku G, Decker C, Charifson P, Weber P, Germann UA *et al* (2007) (S)-1-((S)-2-[1-(4-amino-3-chloro-phenyl)-methanoyl]-amino-3,3-dimethyl-butanoyl)-pyrrolidine-2-carboxylic acid ((2R,3S)-2-ethoxy-5-oxo-tetrahydro-furan-3-yl)-amide (VX-765), an orally available selective interleukin (IL)-converting enzyme/caspase-1 inhibitor, exhibits potent anti-inflammatory activities by inhibiting the release of IL-1beta and IL-18. *J Pharmacol Exp Ther* 321: 509-516

Xiao L, Magupalli VG, Wu H (2023) Cryo-EM structures of the active NLRP3 inflammasome disc. *Nature* 613: 595-600

Xu H, Yang J, Gao W, Li L, Li P, Zhang L, Gong YN, Peng X, Xi JJ, Chen S *et al* (2014) Innate immune sensing of bacterial modifications of Rho GTPases by the Pyrin inflammasome. *Nature* 513: 237-241

Xu J, Nunez G (2023) The NLRP3 inflammasome: activation and regulation. *Trends Biochem Sci* 48: 331-344

Yin H, Guo Q, Li X, Tang T, Li C, Wang H, Sun Y, Feng Q, Ma C, Gao C *et al* (2018) Curcumin Suppresses IL-1beta Secretion and Prevents Inflammation through Inhibition of the NLRP3 Inflammasome. *J Immunol* 200: 2835-2846

Yu X, Matico RE, Miller R, Chauhan D, Van Schoubroeck B, Grauwen K, Suarez J, Pietrak B, Haloi N, Yin Y *et al* (2024) Structural basis for the oligomerization-facilitated NLRP3 activation. *Nat Commun* 15: 1164

Zangiabadi S, Akram A, Abdul-Sater AA (2022) Detection of ASC Oligomerization by Western Blotting. *Methods Mol Biol* 2459: 73-78

Zhang DW, Lazim R (2017) Application of conventional molecular dynamics simulation in evaluating the stability of apomyoglobin in urea solution. *Sci Rep-Uk* 7

Zheng M, Wang P, Song W, Lau SY, Liu S, Huang X, Mok BW, Liu YC, Chen Y, Yuen KY *et al* (2015) An A14U Substitution in the 3' Noncoding Region of the M Segment of Viral RNA Supports Replication of Influenza Virus with an NS1 Deletion by Modulating Alternative Splicing of M Segment mRNAs. *J Virol* 89: 10273-10285

Zhou X, Li G, Kaplan A, Gaschler MM, Zhang X, Hou Z, Jiang M, Zott R, Cremers S, Stockwell BR *et al* (2018) Small molecule modulator of protein disulfide isomerase attenuates mutant huntingtin toxicity and inhibits endoplasmic reticulum stress in a mouse model of Huntington's disease. *Hum Mol Genet* 27: 1545-1555

Figure legends

Fig 1 LOC14 inhibits canonical NLRP3 inflammasome activation. A Schematic representation of the high-throughput screening procedure used to identify potential inhibitors of NLRP3 inflammasome activation. **B** Heatmap depicting the efficiency of 1,140 drugs in inhibiting cell death induced by LPS plus nigericin, indicated by the % of inhibition relative to untreated BMDMs, quantified by propidium iodide. **C, D** Real-time analysis (**C**) and representative images of cell death at 0 h and 1.5 h (**D**) in LOC14 or CRID3-treated wild-type (WT) and *Nlrp3*$^{-/-}$ bone marrow-derived macrophages (BMDMs) stimulated with LPS plus nigericin. Scale bar, 100 μm. **E** Immunoblot analysis of pro- (P45) and cleaved (P20) CASP1, pro- (P53) and cleaved (P30) GSDMD, LDH, and HMGB1 in WT and *Nlrp3*$^{-/-}$ BMDMs stimulated with LPS plus nigericin, with or without LOC14 or CRID3. **F** Measurement of IL-1β release in WT and *Nlrp3*$^{-/-}$ BMDMs stimulated with LPS plus nigericin, with or without LOC14 or CRID3. **G** Immunoblot analysis of pro- (P45) and cleaved (P20) CASP1, and pro- (P53) and cleaved (P30) GSDMD in WT and *Nlrp3*$^{-/-}$ BMDMs treated with LPS plus imiquimod (IMQ), with or without LOC14 or CRID13. GAPDH was used as the internal control (**E, G**). Data are representative of at least three independent experiments. Data are shown as mean ± SEM (**C, F**).

Fig 2 LOC14 does not inhibit AIM2 and NLRP1 inflammasome activation. A, B Real-time analysis (**A**) and Immunoblot analysis of pro- (P45) and cleaved (P20) CASP1, and pro- (P53) and cleaved (P30) GSDMD (**B**) in wild-type (WT) and *Aim2*$^{-/-}$ bone marrow-derived macrophages (BMDMs) infected with *Francisella novicida* for 16 h, with or without LOC14. **C, D** Real-time analysis (**C**) and immunoblot analysis of pro- (P45) and cleaved (P20) CASP1, and pro- (P53) and cleaved (P30) GSDMD (**D**) in WT and *Aim2*$^{-/-}$ BMDMs transfected with poly(dA:dT) for 4 h, with or without LOC14. **E–G** Real-time analysis (**E**), representative images of cell death at 0 h and 16 h (**F**), and

immunoblot analysis of pro- (P45) and cleaved (P20) CASP1, and pro- (P53) and cleaved (P30) GSDMD in WT BMDMs treated with Val-boroPro for 16 h (**G**), with or without LOC14. Scale bar, 100 μm. GAPDH was used as the internal control (**B, D, G**). Data are representative of at least three independent experiments. Data are shown as mean ± SEM (**A, C, E**).

Fig 3 LOC14 suppresses inflammasome activation by targeting NLRP3 and NEK7. A, B Semi-denaturing detergent agarose gel electrophoresis (SDD-AGE) indicating NLRP3 oligomers (**A**) and Sodium dodecyl-sulfate polyacrylamide gel electrophoresis (SDS-PAGE) indicating ASC oligomers (**B**) in LOC14-treated wild-type (WT) or *Nlrp3*$^{-/-}$ bone marrow-derived macrophages (BMDMs) following stimulation with LPS plus ATP for 30 min and LPS plus nigericin for 1 h. **C** Glide extra precision (XP) Gscore analysis from molecular docking of LOC14 and CRID3 binding to NLRP3, with or without NEK7. **D** Immunoblot analysis of NLRP3, CASP1, and ASC in LPS-primed bone marrow-derived macrophages (BMDMs) treated with or without LOC14 and pronase. **E** Immunoblot analysis of Flag in HEK293T cells expressing full-length NLRP3 treated with or without LOC14 and pronase. **F** An NLRP3 target engagement assay using HEK293FT cells treated with a concentration of 0.05, 0.5, 1, 5, 10, 15, 20 and 40 μM of LOC14, CRID3, or qVD. The normalized Bioluminescence Resonance Energy Transfer (BRET) signal indicates the % of the signal from the NanoBRET tracer on NLRP3 that were being displaced by the inhibitors. The half maximal inhibitory concentration (IC50) indicates the concentration of inhibitor required to reduce the NanoBRET tracer signal by 50%. Each symbol represents an individual concentration. **G** Immunoblot analysis of NEK7 and NLRP3 following immunoprecipitation (IP) with anti-NLRP3 or IgG control antibodies in LPS-primed THP1 cells treated with nigericin, with or without LOC14 (5 μM). GAPDH (**B**) and β-actin (**D, E, G**) were used as internal controls. Data are representative of two to three independent experiments.

Fig 4 LOC14 binds the LRR domain of NLRP3. A Schematic of the different domains of NLRP3 overexpressed in HEK293T cells. **B, C** Immunoblot analysis of Flag in HEK293T cells expressing either LRR (**B**), NACHT, or PYD (**C**) domains of NLRP3, treated with or without LOC14 (5 μM) and pronase. **D, E** Molecular docking of LOC14 with NLRP3-NEK7 (6NPY): 3D representation (**D**) and 2D representation (**E**) showing ligand interactions via H-bonds and hydrophobic interactions with the active site of the protein. β-actin was used as the internal control (**B, C**). Data are representative of at least three independent experiments.

Fig 5 Isothiazol-3(2H)-one moiety is the inhibitory component of LOC14. A Chemical structures of LOC14, 1,2-Benisothiazol-3(2H)-one (BITO) and 1-(cyclopropylcarbonyl)piperazine-3(2H)-one (PCP). **B, C** Percentage of cell death (**B**) and immunoblot analysis of pro- (P45) and cleaved (P20) CASP1, and pro- (P53) and cleaved (P30) GSDMD in wild type (WT) bone marrow-derived macrophages (BMDMs) stimulated with LPS plus nigericin for 1 h (**C**), with or without LOC14, BITO, or PCP. **D** Chemical structures of isothiazol-3(2H)-one (ITO), isothiazole (IT), thiazole (T), or imidazole (I). **E, F** Real-time analysis (**E**) and representative images of cell death in WT BMDMs stimulated with LPS plus nigericin for 1 h (**F**), without or without ITO, IT, T, or I. Scale bar, 100 μm. **G** Immunoblot analysis of pro- (P45) and cleaved (P20) CASP1, and pro- (P53) and cleaved (P30) GSDMD in WT BMDMs stimulated with LPS plus nigericin for 1 h, with or without ITO, IT, T, or I. **H** IC50 values of LOC14, BITO, ITO, or CRID3 in inhibiting cell death triggered by LPS plus nigericin for 1 h. GAPDH was used as the internal control (**C, G**). Data are representative of at least three independent experiments. Data are shown as mean ± SEM (**B, E, H**).

Fig 6 LOC14 inhibits the priming step of the NLRP3 inflammasome. A, B Immunoblot analysis of ASC, NLRP3, and pro-IL-1β (**A**), and phosphorylated IκBα (p-IκBα), total p-IκBα (t-IκBα), phosphorylated ERK1/2 (p-ERK), total ERK1/2 (t-ERK), phosphorylated JNK (p-JNK), and total JNK (t-JNK) (**B**) in LPS-stimulated WT BMDMs treated with LOC14 for the indicated times. **C, D** Immunoblot analysis of ASC, NLRP3, and pro-IL-1β (**C**), and phosphorylated IκBα (p-IκBα), total IκBα (t-IκBα), phosphorylated ERK1/2 (p-ERK), total ERK1/2 (t-ERK), phosphorylated JNK (p-JNK), and total JNK (t-JNK) (**D**) in Pam3CSK4 (Pam3)-stimulated WT BMDMs treated with LOC14 for the indicated times. GAPDH (**B**) and β-actin (**A, C, D**) were used as internal controls. Data are representative of at least three independent experiments.

Fig 7 LOC14 ameliorates DSS-induced colonic inflammation in mice. A Body weight change of wild-type (WT) mice administered with vehicle or LOC14 during dextran sulfate sodium (DSS) treatment. **B** Representative images of the colon from WT mice administered with vehicle or LOC14, 9 days after DSS administration. **C** Levels of IL-1β and IL-18 in colons of WT mice administered with vehicle or LOC14, 9 days after DSS administration. **D** Representative hematoxylin and eosin (H&E) staining of colon sections. Scale bar, 100 μm. Sections include a whole scan and specific regions (proximal, middle, and distal colon). Each symbol represents an individual mouse (**C**). Data are shown as mean ± SEM (**A, C**). *$P < 0.05$, and ***$P < 0.001$. One-way ANOVA (**A**); and two-way ANOVA (**C**). Data are from one experiment representative of two independent experiments (**A–D**).

Fig 8 LOC14 alleviates IMQ-induced skin inflammation in mice. A Representative images of mice developing psoriasis-like skin inflammation, 6 days after Aldara application and 5 days after administration of LOC14 or CRID3. **B** Psoriasis area and severity index (PASI) in mice, 6 days after Aldara application. Each symbol

represents an individual mouse. **C** Representative hematoxylin and eosin (H&E) staining of skin sections. Scale bar, 100 μm. **D** Measurement of epidermal thickness of skin sections in (**C**). **E** Immunoblot analysis of pro- (P53) and cleaved (P30) GSDMD in the skin of mice, 6 days after Aldara application. β-actin was used as the internal control. Data are shown as mean ± SEM (**B, D**). $^{**}P < 0.01$, $^{***}P < 0.001$, and $^{****}P < 0.0001$; one-way ANOVA (**B, D**). Data are from one experiment representative of two independent experiments (**A–E**).

Supplemental figure legends

Supplementary Figure 1. LOC14 inhibits the canonical NLRP3 inflammasome. **a, b,** Real-time analysis (a) and representative images of cell death at 0 h and 1.5 h (B) in LPS-primed wild type (WT) and *Nlrp3*$^{-/-}$ bone marrow-derived macrophages (BMDMs) stimulated with ATP plus LOC14 or CRID3. Scale bar, 100 μm. **c,** Immunoblot analysis of pro- (P45) and cleaved (P20) CASP1, pro- (P53) and cleaved (P30) GSDMD, and LDH in LPS-primed WT and *Nlrp3*$^{-/-}$ BMDMs with or without LOC14 or CRID3, 1 h after ATP stimulation. **d,** IL-1β release in LPS-primed WT and *Nlrp3*$^{-/-}$ BMDMs treated with ATP plus LOC14 or CRID3 for 1 h. **e,** Immunoblot analysis of cleaved CASP1 and GSDMD from supernatants or full-length CASP1 and GSDMD from cell lysates of LPS-primed THP1 cells treated with nigericin plus LOC14 or CRID3 for 1 h. **f,** Immunoblot analysis of cleaved CASP1 p20 and GSDMD p30 of primary peripheral blood mononuclear cells (PBMCs) from three healthy human donors treated with Pam3CSK4 for 2.5 h followed by 1.5 h nigericin in the presence of DMSO, LOC14 or CRID3. **g,** IL-1β release from primary human PBMCs as in F, with each symbol representing an individual healthy human donor. GAPDH (c) and β-actin (e, f) were used as internal controls. ****$P < 0.0001$; one-way ANOVA (g). Data are representative of at least three independent experiments. Data are shown as mean ± SEM (a, d, g).

Supplementary Figure 2. PDIA3 is not required for NLRP3 inflammasome activation. a, b, Cell death rate and representative images (a) and immunoblot analysis of PDIA3, pro- (P45) and cleaved (P20) CASP1, and pro- (P53) and cleaved (P30) GSDMD (b) in PDIA3 or control siRNA-transfected BMDMs stimulated with LPS plus ATP for 0.5 h. **c, d,** Cell death rate and representative images (c) and immunoblot analysis of PDIA3, pro- (P45) and cleaved (P20) CASP1, and pro- (P53) and cleaved (P30) GSDMD (d) in PDIA3 or control siRNA-transfected BMDMs stimulated with LPS

plus nigericin for 1 h. **e, f,** Immunoblot analysis of phosphorylated IκBα (p-IκBα), total IκBα (t-IκBα), phosphorylated ERK1/2 (p-ERK), total ERK1/2 (t-ERK), phosphorylated JNK (p-JNK), and total JNK (t-JNK) (e) and NLRP3, pro-IL-1β, and PDIA3 (f) in LPS-stimulated WT BMDMs upon transfection with PDIA3 or control siRNA. GAPDH (b, d) and β-actin (e, f) were used as internal controls. Data are representative of at least three independent experiments. Data are shown as mean ± SEM (a, c).

Supplementary Figure 3. LOC14 inhibits the non-canonical NLRP3 inflammasome. a, Immunoblot analysis of pro- (P45) and cleaved (P20) CASP1, pro- (P53) and cleaved (P30) GSDMD, and LDH in LPS-transfected WT BMDMs treated with LOC14 or CRID3 for 6 h. **b,** IL-1β release in WT BMDMs 6 h after LPS transfection, with or without LOC14 or CRID3. **c, d,** Real-time analysis (c) and representative images of cell death at 0 h and 6 h (d) in LPS-transfected WT BMDMs with or without LOC14. Scale bar, 100 μm. GAPDH was used as an internal control (a). Data are representative of at least three independent experiments. Data are shown as mean ± SEM (b, c).

Supplementary Figure 4. LOC14 does not affect AIM2, NLRC4 and Pyrin inflammasome activation. a, b, Immunoblot analysis of IRF1 in wild-type (WT) bone marrow-derived macrophages (BMDMs) infected with 100 MOI of *Francisella novicida* (a) and stimulated with IFN-β (b) in the presence of LOC14 for the indicated times. **c, d,** Real-time analysis (c) and immunoblot analysis of pro- (P45) and cleaved (P20) CASP1, and pro- (P53) and cleaved (P30) GSDMD (d) in WT and *Nlrc4*$^{-/-}$ BMDMs infected with 1 MOI of *Salmonella enterica* subspecies *enterica* serovar Typhimurium for 6 h in the presence of LOC14. **e, f,** Real-time analysis (e) and immunoblot analysis of pro- (P45) and cleaved (P20) CASP1, and pro- (P53) and cleaved (P30) GSDMD (f) in WT and *Mefv*$^{-/-}$ BMDMs incubated with *Clostridium difficile* supernatant for 20 h in the presence

of LOC14. GAPDH was used as the internal control (a, b, d, f). Data are representative of at least three independent experiments. Data are shown as mean ± SEM (c, e).

Supplementary Figure 5. LOC14 reduces ASC speck formation in LPS-primed THP1-ASC-GFP cells. Fluorescence microscopy images of LPS-primed THP1-ASC-GFP cells treated with nigericin plus LOC14 or CRID3 for 1 h. Scale bar, 50 μm. Data are representative of at least three independent experiments.

Supplementary Figure 6. LOC14 exhibits a higher degree of spontaneity in its interaction with NLRP3-NEK7. a, b, Structural analysis of NLRP3-NEK7 active site. **c,** MM/GBSA profiles of LOC14 in interaction with NLRP3 bound to NEK7.

Supplementary Figure 7. LOC14 protects NLRP3 from proteolysis. a, Immunoblot analysis of NLRP3 in HEK293T cells overexpressing mouse-NLRP3 treated with or without LOC14 and pronase. **b,** Immunoblot analysis of Flag in HEK293T cells expressing human-NLRP6 treated with or without LOC14 and pronase. β-actin was used as the internal control (a, b). Data are representative of at least three independent experiments.

Supplementary Figure 8. LOC14 inhibits cell death induced by NLRP3 mutants associated with cryopyrin-associated periodic syndrome. a, b, Human monocytic cell line U937 expressing doxycycline-inducible NLRP3 gain-of-function mutants associated with cryopyrin-associated periodic syndrome, (a) D303H and (b) K568N, were treated with the vehicle control DMSO or LOC14. **c,** IL-1β release in primary peripheral blood mononuclear cells (PBMCs) from a human patient with cryopyrin-associated periodic syndrome and the NLRP3 gain-of-function mutant R490K, left untreated or treated with LPS for 6 h in the presence of LOC14 or CRID3.

Data represent one of two independent experiments (a, b), or pooled from three independent fresh blood samples taken from the same human patient (c). **P < 0.01; ***P < 0.001; one-way ANOVA (a-c).

Supplementary Figure 9. Isothiazol-3(2H)-one moiety inhibits the NLRP3 inflammasome. a, Percentage of cell death in WT BMDMs stimulated with LPS plus nigericin for 1 h with or without ITO, benzisothiazol-3(2H)-one (BITO), or LOC14 at a concentration of 2 μM. **b,** Immunoblot analysis of pro- (P45) and cleaved (P20) CASP1, and pro- (P53) and cleaved (P30) GSDMD in influenza A virus (IAV)-infected wild type (WT) and *Nlrp3*$^{-/-}$ bone marrow-derived macrophages (BMDMs) treated with or without isothiazol-3(2H)-one (ITO) or CRID3 for 16 h. **c, e,** Real-time analysis and **d, f,** representative images of cell death at 0 h and 1.5 h in LPS-primed WT BMDMs stimulated with ATP plus (c,d) 4,5-dichloro-2-n-octyl-4-isothiazoline-3-one (DCOIT) or (e, f) methylisothiazolinone (M-ITO). Scale bar, 100 μm. GAPDH was used as the internal control (b). Data are representative of at least three independent experiments. Data are shown as mean ± SEM (a, c, e).

Supplementary Figure 10. LOC14 inhibits NLRP3 inflammasome priming. a, Schematic diagram showing LOC14 treatment during priming or activation events of NLRP3 inflammasome activation. **b,** Real-time analysis of cell death in LPS plus LOC14- or CRID3-treated wild-type (WT) and *Nlrp3*$^{-/-}$ bone marrow-derived macrophages (BMDMs) with nigericin stimulation after 4 h. **c,** IL-1β release in LPS plus LOC14- or CRID3-treated WT and *Nlrp3*$^{-/-}$ BMDMs with nigericin stimulation after 4 h for 1 h. **d,** Immunoblot analysis of pro- (P45) and cleaved (P20) CASP1 and pro- (P53) and cleaved (P30) GSDMD in LPS plus LOC14-or CRID3-treated WT and *Nlrp3*$^{-/-}$ BMDMs with nigericin stimulation after 4 h for 1 h. **e,** Real-time analysis of cell death in LPS plus

LOC14- or CRID3-treated WT and *Nlrp3*$^{-/-}$BMDMs with ATP stimulation after 4 h. **f,** IL-1β release in LPS plus ATP- or CRID3-treated WT and *Nlrp3*$^{-/-}$ BMDMs with ATP stimulation after 4 h for 1h. **g,** Immunoblot analysis of pro- (P45) and cleaved (P20) CASP1 and pro- (P53) and cleaved (P30) GSDMD in LPS plus LOC14- or CRID3-treated WT and *Nlrp3*$^{-/-}$ BMDMs with ATP stimulation after 4 h for 1 h. GAPDH was used as the internal control (d, g). Data are representative of at least three independent experiments. Data are shown as mean ± SEM (b, c, e, f).

Supplementary Figure 11. LOC14 delays priming of NLRP3. a, RT-PCR analysis of Nlrp3 expression in wild-type (WT) bone-marrow-derived macrophages (BMDMs) stimulated with LPS, Pam3CSK4 (Pam3), or Poly I:C (I:C) in the presence of LOC14 for the indicated times. **b, c,** Immunoblot analysis of ASC, NLRP3, and pro-IL-1β (b) and phosphorylated IκBα (p-IκBα), total IκBα (t-IκBα), phosphorylated ERK1/2 (p-ERK), total ERK1/2 (t-ERK), phosphorylated JNK (p-JNK), and total JNK (t-JNK) (c) in WT BMDMs stimulated with I:C in the presence of LOC14 for the indicated times. **d,** Immunoblot analysis of NLRP3 and pro-IL-1β in LPS-stimulated BMDMs treated with ITO, BITO or LOC14 at a concentration of 2 μM for the indicated times. **e,** Immunoblot analysis of phosphorylated IκBα (p-IκBα), total IκBα (t-IκBα), phosphorylated ERK1/2 (p-ERK), total ERK1/2 (t-ERK), phosphorylated JNK (p-JNK), and total JNK (t-JNK) in LPS-stimulated WT BMDMs in the presence of ITO, BITO, or LOC14 at a concentration of 2 μM for the indicated times. GAPDH (b) and β-actin (c-e) were used as internal controls. Data are representative of at least three independent experiments. Data are shown as mean ± SEM (a).

Supplementary Figure 12. LOC14 inhibits inflammatory responses in mice. a, Colon length of wild-type (WT) mice administered with vehicle or LOC14, 9 days after

dextran sulfate sodium (DSS) administration. **b,** Levels of IL-1β in the serum of WT mice administered with vehicle or LOC14, 4 h after LPS injection. Each symbol represents an individual mouse (a, b). Data are shown as mean ± SEM (a, b). **P < 0.01, and ***P < 0.001; two-way ANOVA (a), two-tailed t-test (b). Data are from one experiment representative of two independent experiments (a, b).

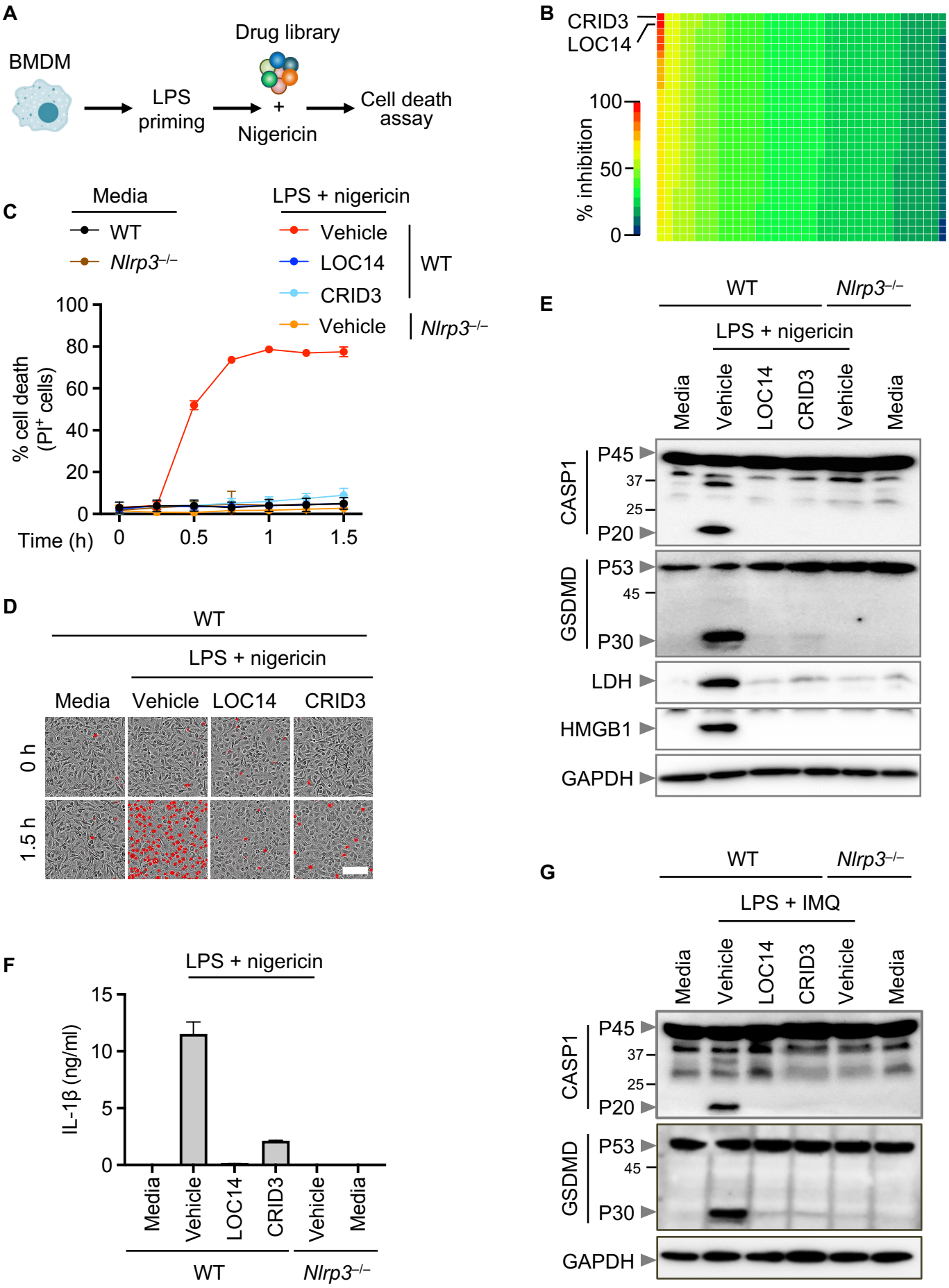
A
BMDM
LPS priming
Drug library
+
Nigericin
Cell death assay
B
CRID3
LOC14
100
50
0
% inhibition
C
Media
WT
Nlrp3−/−
LPS + nigericin
Vehicle
LOC14
CRID3
Vehicle
WT
Nlrp3−/−
% cell death (PI+ cells)
100
80
60
40
20
0
Time (h)
0
0.5
1
1.5
D
WT
LPS + nigericin
Media
Vehicle
LOC14
CRID3
0 h
1.5 h
E
WT
Nlrp3−/−
LPS + nigericin
Media
Vehicle
LOC14
CRID3
Vehicle
Media
CASP1
P45
37
25
P20
GSDMD
P53
45
P30
LDH
HMGB1
GAPDH
F
LPS + nigericin
IL-1β (ng/ml)
15
10
5
0
Media
Vehicle
LOC14
CRID3
Vehicle
Media
WT
Nlrp3−/−
G
WT
Nlrp3−/−
LPS + IMQ
Media
Vehicle
LOC14
CRID3
Vehicle
Media
CASP1
P45
37
25
P20
GSDMD
P53
45
P30
GAPDH

Figure 1

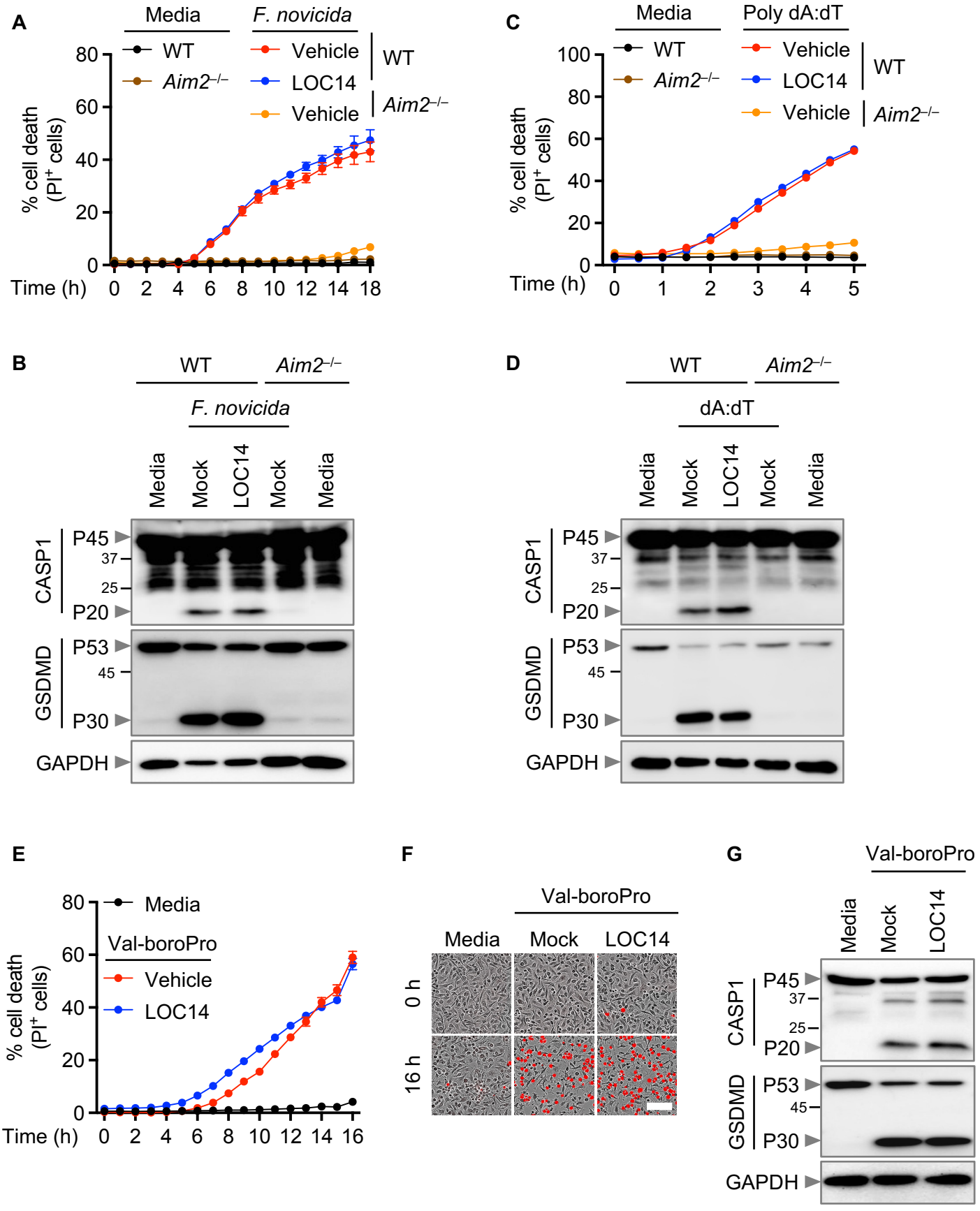
A
Media
F. novicida
WT
Aim2−/−
Vehicle
LOC14
Vehicle
WT
Aim2−/−
% cell death (PI+ cells)
Time (h)
C
Media
Poly dA:dT
WT
Aim2−/−
Vehicle
LOC14
Vehicle
WT
Aim2−/−
% cell death (PI+ cells)
Time (h)
B
WT
Aim2−/−
F. novicida
Media
Mock
LOC14
Mock
Media
CASP1
P45
37
25
P20
GSDMD
P53
45
P30
GAPDH
D
WT
Aim2−/−
dA:dT
Media
Mock
LOC14
Mock
Media
CASP1
P45
37
25
P20
GSDMD
P53
45
P30
GAPDH
E
Media
Val-boroPro
Vehicle
LOC14
% cell death (PI+ cells)
Time (h)
F
Val-boroPro
Media
Mock
LOC14
0 h
16 h
G
Val-boroPro
Media
Mock
LOC14
CASP1
P45
37
25
P20
GSDMD
P53
45
P30
GAPDH

Figure 2

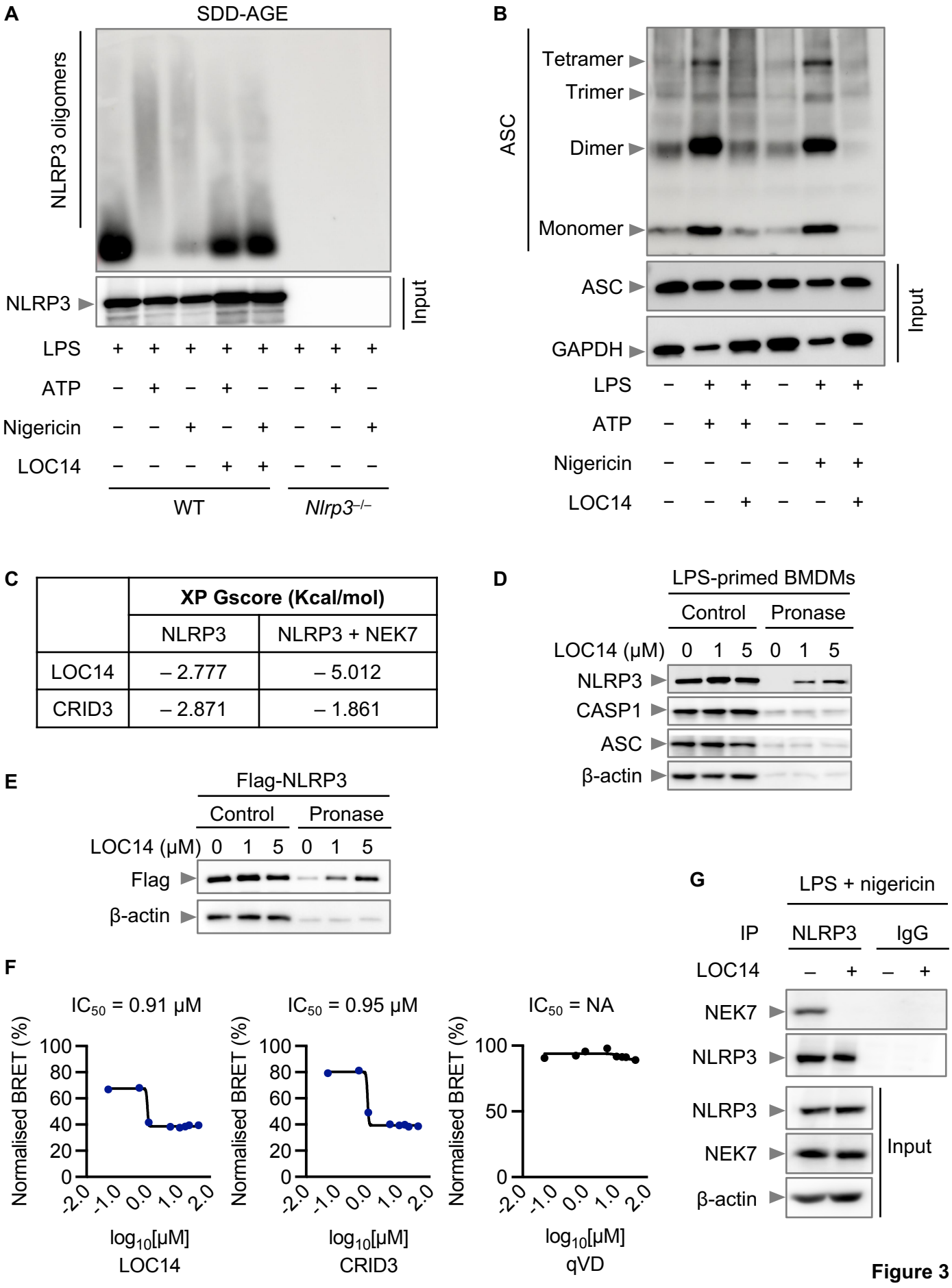
A
SDD-AGE
NLRP3 oligomers
NLRP3
Input
LPS + + + + + + + +
ATP – + – + – – + –
Nigericin – – + – + – – +
LOC14 – – – + + – – –
WT
Nlrp3–/–
B
Tetramer
Trimer
Dimer
Monomer
ASC
ASC
GAPDH
Input
LPS – + + – + +
ATP – + + – – –
Nigericin – – – – + +
LOC14 – – + – – +
C
XP Gscore (Kcal/mol)
NLRP3
NLRP3 + NEK7
LOC14 – 2.777 – 5.012
CRID3 – 2.871 – 1.861
D
LPS-primed BMDMs
Control
Pronase
LOC14 (μM) 0 1 5 0 1 5
NLRP3
CASP1
ASC
β-actin
E
Flag-NLRP3
Control
Pronase
LOC14 (μM) 0 1 5 0 1 5
Flag
β-actin
F
IC50 = 0.91 μM
IC50 = 0.95 μM
IC50 = NA
Normalised BRET (%)
100
80
60
40
20
0
50
-2.0
-1.0
0.0
1.0
2.0
log10[μM]
LOC14
CRID3
qVD
G
LPS + nigericin
IP
NLRP3
IgG
LOC14 – + – +
NEK7
NLRP3
NLRP3
NEK7
β-actin
Input

Figure 3

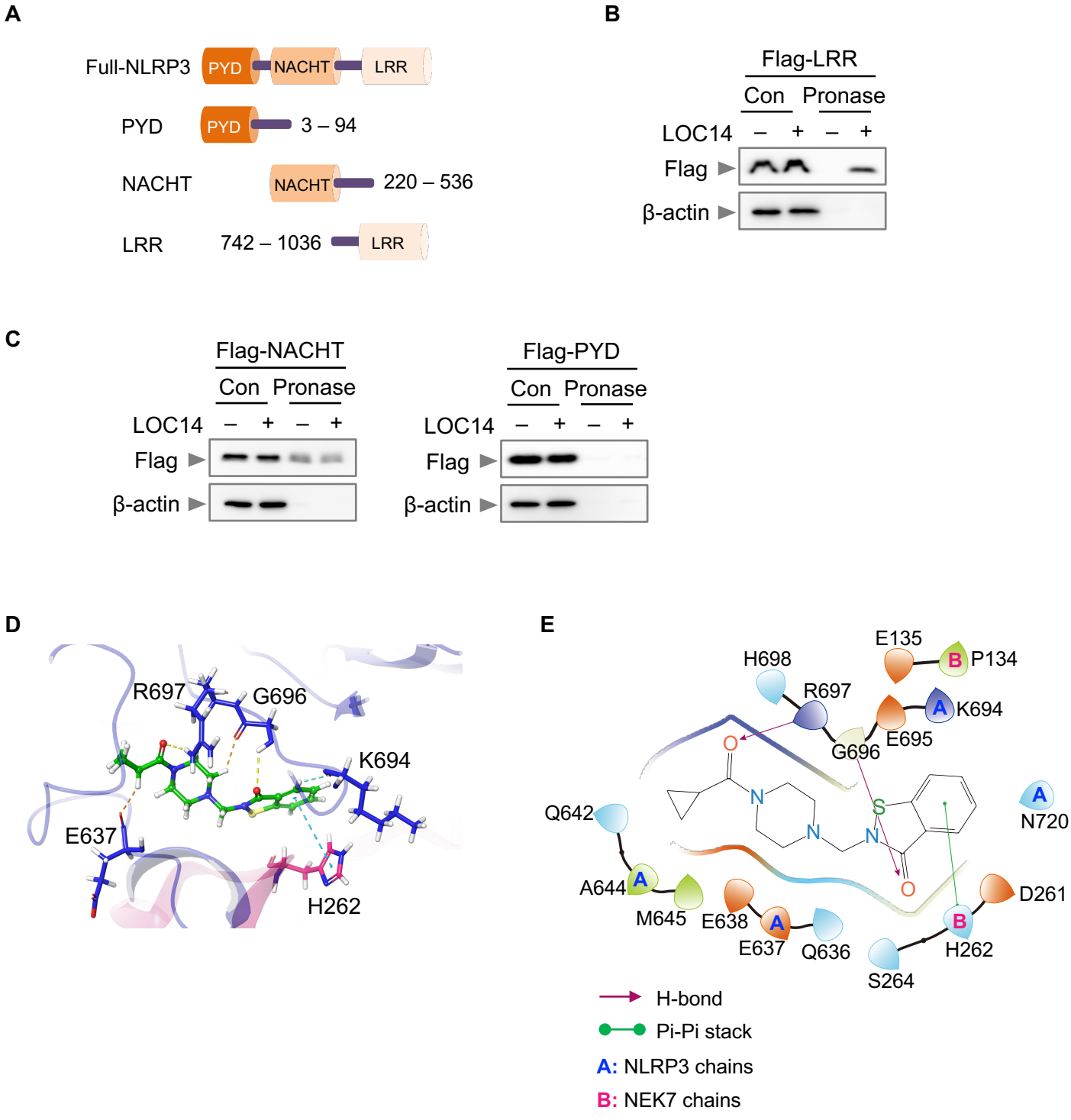
A
Full-NLRP3
PYD
NACHT
LRR
PYD
PYD
3 – 94
NACHT
NACHT
220 – 536
LRR
742 – 1036
LRR
B
Flag-LRR
Con
Pronase
LOC14 – + – +
Flag
β-actin
C
Flag-NACHT
Con
Pronase
LOC14 – + – +
Flag
β-actin
Flag-PYD
Con
Pronase
LOC14 – + – +
Flag
β-actin
D
R697
G696
K694
E637
H262
E
E135
P134
H698
R697
K694
E695
G696
Q642
N720
A644
M645
E638
E637
Q636
D261
H262
S264
H-bond
Pi-Pi stack
A: NLRP3 chains
B: NEK7 chains

Figure 4

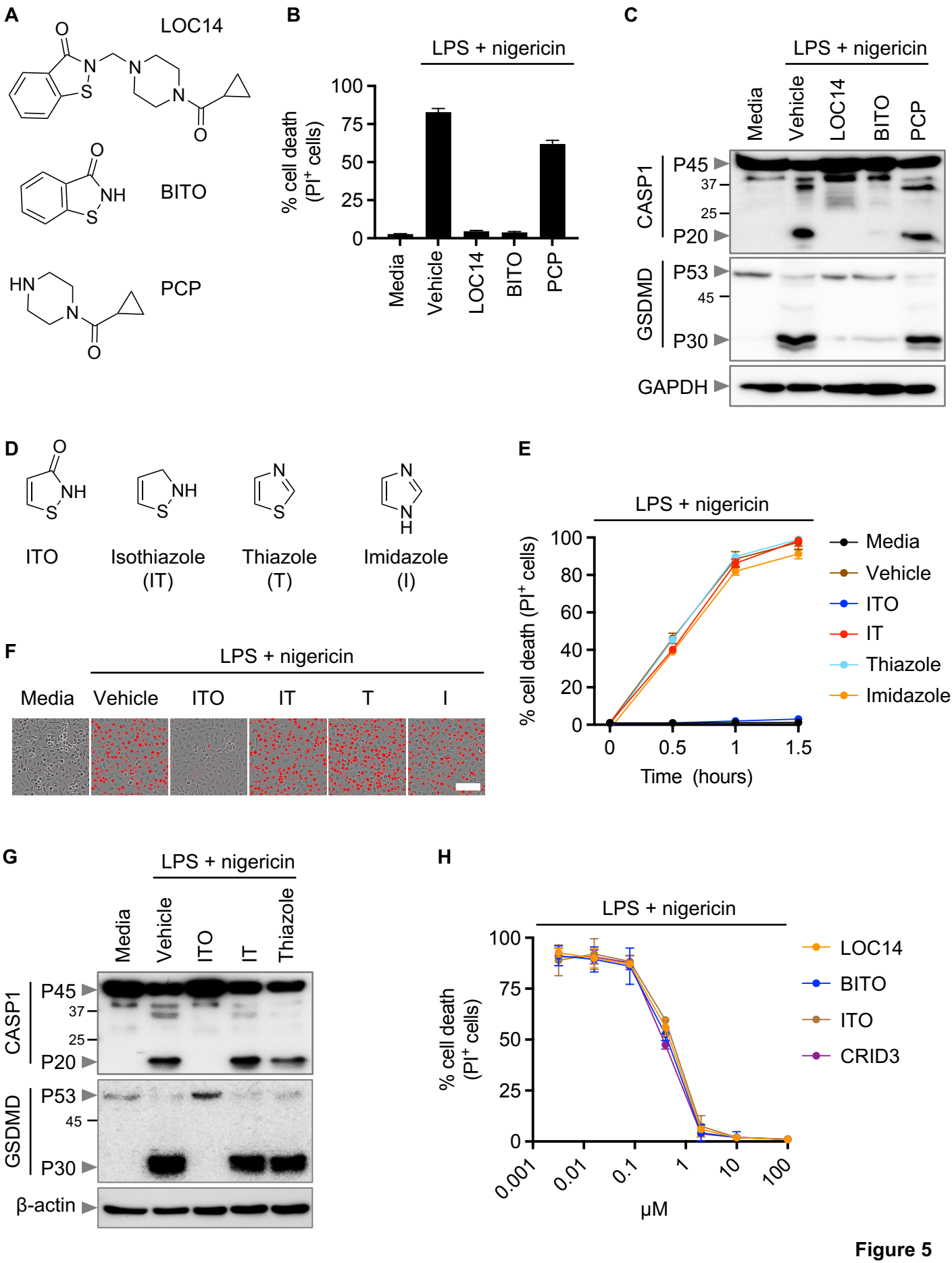
A
LOC14
BITO
PCP
B
LPS + nigericin
% cell death (PI+ cells)
100
75
50
25
0
Media
Vehicle
LOC14
BITO
PCP
C
LPS + nigericin
Media
Vehicle
LOC14
BITO
PCP
CASP1
P45
37
25
P20
GSDMD
P53
45
P30
GAPDH
D
ITO
Isothiazole (IT)
Thiazole (T)
Imidazole (I)
E
LPS + nigericin
% cell death (PI+ cells)
100
80
60
40
20
0
0
0.5
1
1.5
Time (hours)
Media
Vehicle
ITO
IT
Thiazole
Imidazole
F
LPS + nigericin
Media
Vehicle
ITO
IT
T
I
G
LPS + nigericin
Media
Vehicle
ITO
IT
Thiazole
CASP1
P45
37
25
P20
GSDMD
P53
45
P30
β-actin
H
LPS + nigericin
% cell death (PI+ cells)
100
75
50
25
0
0.001
0.01
0.1
1
10
100
μM
LOC14
BITO
ITO
CRID3

Figure 5

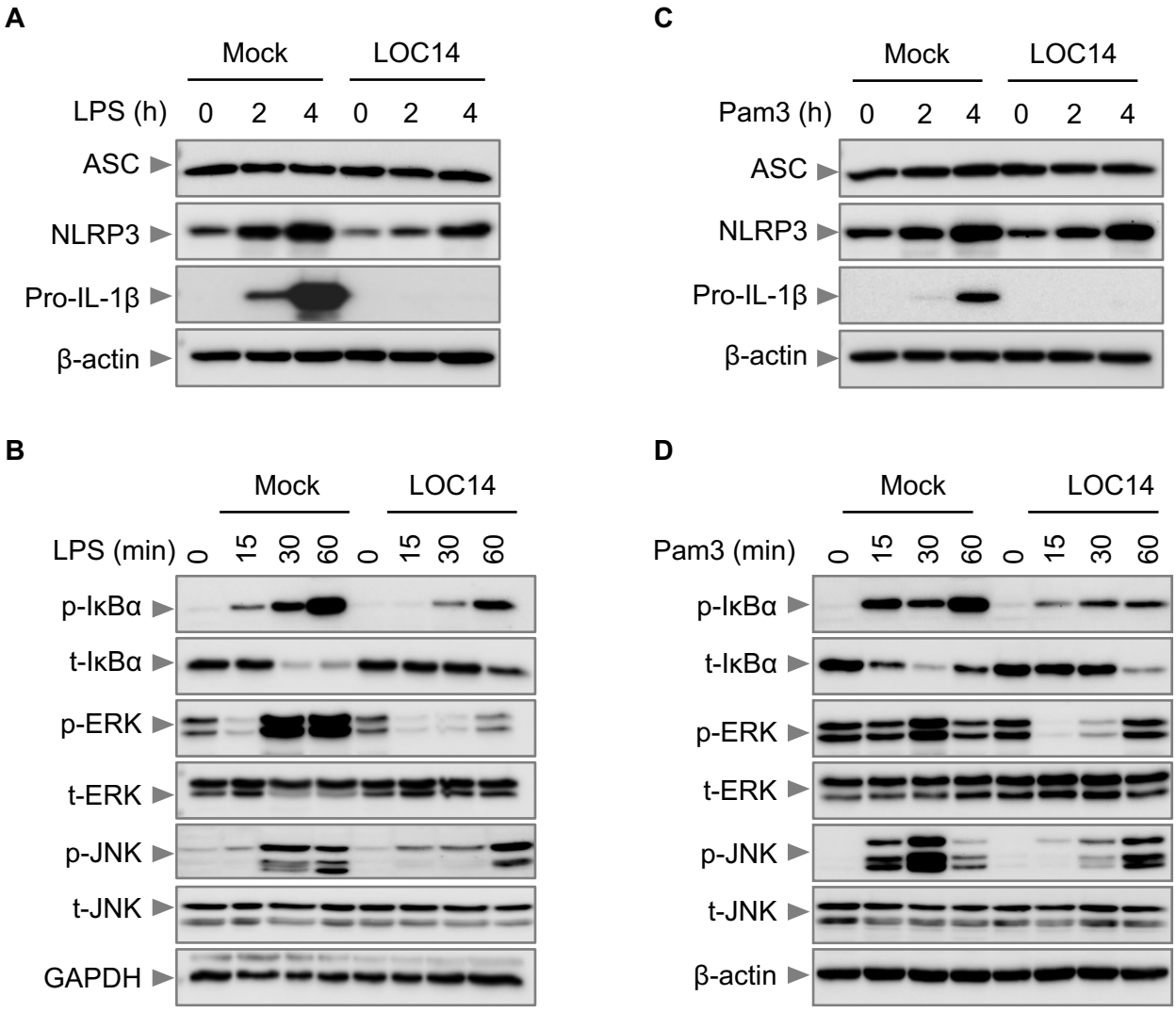
A
Mock
LOC14
LPS (h)
0 2 4 0 2 4
ASC
NLRP3
Pro-IL-1β
β-actin
C
Mock
LOC14
Pam3 (h)
0 2 4 0 2 4
ASC
NLRP3
Pro-IL-1β
β-actin
B
Mock
LOC14
LPS (min)
0 15 30 60 0 15 30 60
p-IκBα
t-IκBα
p-ERK
t-ERK
p-JNK
t-JNK
GAPDH
D
Mock
LOC14
Pam3 (min)
0 15 30 60 0 15 30 60
p-IκBα
t-IκBα
p-ERK
t-ERK
p-JNK
t-JNK
β-actin

Figure 6

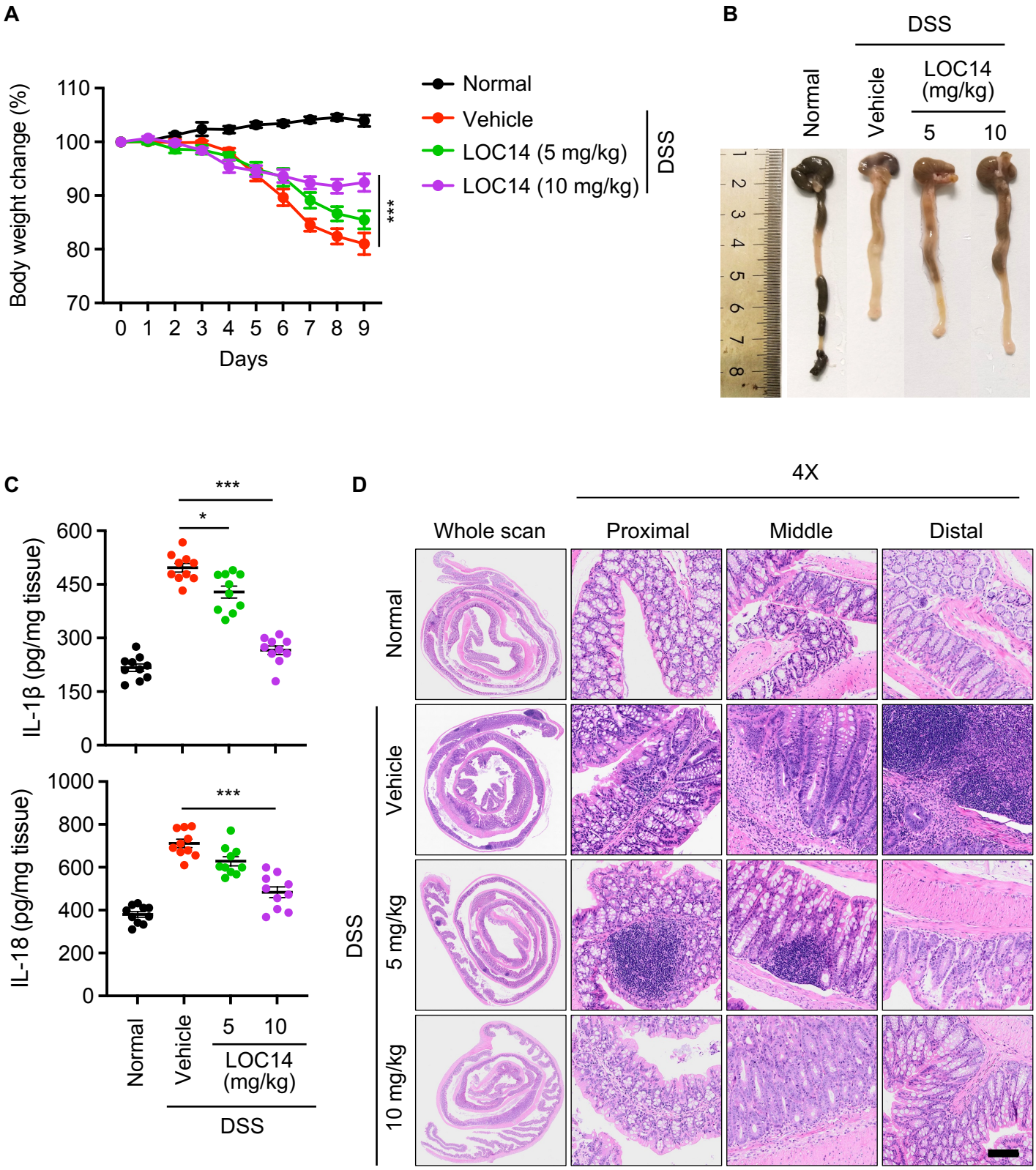
A
Body weight change (%)
110
100
90
80
70
0 1 2 3 4 5 6 7 8 9
Days
Normal
Vehicle
LOC14 (5 mg/kg)
LOC14 (10 mg/kg)
DSS
***
B
DSS
Normal
Vehicle
LOC14 (mg/kg)
5
10
C
IL-1β (pg/mg tissue)
600
450
300
150
0
***
*
IL-18 (pg/mg tissue)
1000
800
600
400
200
0
***
Normal
Vehicle
5
10
LOC14 (mg/kg)
DSS
D
4X
Whole scan
Proximal
Middle
Distal
Normal
Vehicle
5 mg/kg
10 mg/kg
DSS

Figure 7

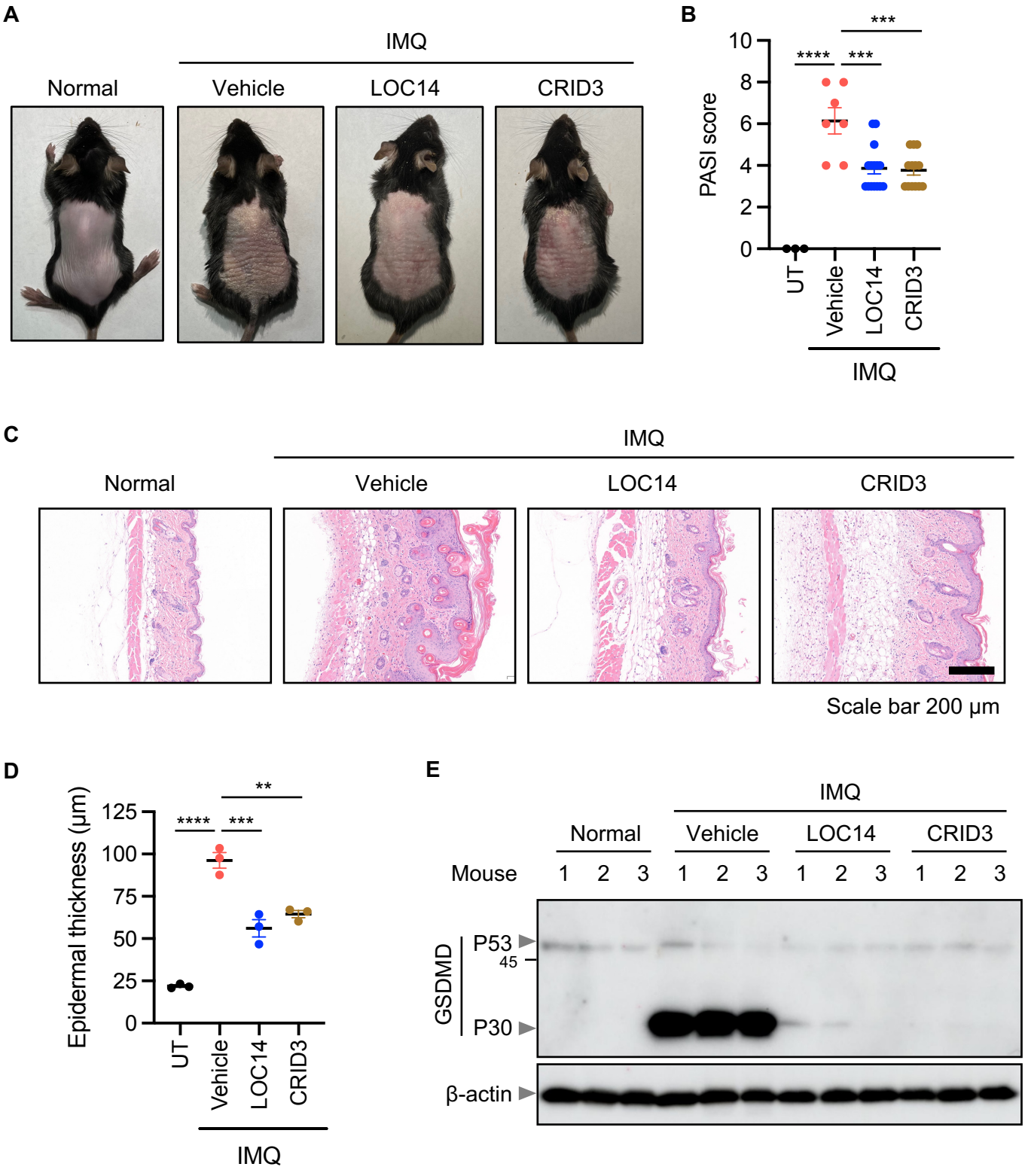
A
IMQ
Normal
Vehicle
LOC14
CRID3
B
PASI score
10
8
6
4
2
0
****
***
***
UT
Vehicle
LOC14
CRID3
IMQ
C
IMQ
Normal
Vehicle
LOC14
CRID3
Scale bar 200 μm
D
Epidermal thickness (μm)
125
100
75
50
25
0
**
****
***
UT
Vehicle
LOC14
CRID3
IMQ
E
IMQ
Normal
Vehicle
LOC14
CRID3
Mouse
1 2 3 1 2 3 1 2 3 1 2 3
GSDMD
P53
45
P30
β-actin

Figure 8